Genomic-Thermodynamic Phase Synchronization: Maxwell's Demon-Like Regulation of Cell Fate Transition

Masa Tsuchiya[1]*, Kenichi Yoshikawa[2] and Alessandro Giuliani[3]

[1]SEIKO Life Science Laboratory, SEIKO Research Institute for Education, Osaka, Japan
[2]Faculty of Life and Medical Sciences, Doshisha University, Kyotanabe, Japan
[3]Environment and Health Department, Istituto Superiore di Sanitá (Italian NIH), Rome, Italy

Conflict of Interest: The authors declare no conflict of interest.

*Correspondence: tsuchiya.masa@gmail.com

Abstract

Dynamic criticality - the balance between order and chaos - is fundamental to genome regulation and cellular transitions. In this study, we investigate the distinct behaviors of gene expression dynamics in MCF-7 breast cancer cells under two stimuli: Heregulin (HRG), which promotes cell fate transitions, and Epidermal Growth Factor (EGF), which, despite binding to the same receptor, does not induce cell fate changes. We model the system as an open, non-equilibrium thermodynamic system and introduce a convergence-based approach for robust estimation of information-thermodynamic metrics.

Our analysis reveals that the Shannon entropy of the critical point (CP) dynamically synchronizes with the entropy of the rest of the whole expression system (WES), reflecting coordinated transitions between ordered and disordered phases. This phase synchronization is driven by net mutual information scaling with CP entropy dynamics, demonstrating how the CP governs genome-wide coherence. Furthermore, high-order mutual information emerges as a defining feature of the nonlinear gene expression network, capturing collective effects beyond simple pairwise interactions.

By achieving thermodynamic phase synchronization, the CP orchestrates the entire expression system. Under HRG stimulation, the CP becomes active, functioning as a Maxwell's demon with dynamic, rewritable chromatin memory to guide a critical transition in cell fate. In contrast, under EGF stimulation, the CP remains inactive in this strategic role, passively facilitating a non-critical transition.

These findings establish a biophysical framework for cell fate determination, paving the way for innovative approaches in cancer research and stem cell therapy.

Introduction

Dynamic criticality in gene expression, characterized by shifts in global expression profiles initiated by changes in specific gene subsets, plays a pivotal role in regulating genome dynamics and driving critical transitions [Liu et al., 2017]. The delicate balance between order and chaos enables genomic regulation that is both flexible and stable [Shmulevich et al., 2005; Zimatore et al., 2021].

Our previous studies demonstrated that this balance underlies both precise cellular responses to external signals and fundamental processes such as cell differentiation and embryonic development. These dynamics are central to understanding cell fate changes. Our key findings are summarized below:

1. **Emergent Self-Organization within a Genome Attractor**
   Self-organized critical (SOC) control of genome expression is quantified by the Normalized Root Mean Square Fluctuation *(nrmsf)*, which delineates distinct response domains (critical states). Large gene groups exhibit Coherent Stochastic Behavior (CSB), converging around centers of mass (CM), treated as unit masses, that act as attractors [Tsuchiya et al., 2014, 2015, 2016]. The whole genome CM is the Genome Attractor (GA), while local critical states serve as subcritical or supercritical attractors. Cyclic fluxes among these attractors create an open thermodynamic "genome engine" that regulates genome expression [Tsuchiya et al., 2020, 2022].
2. **CP as a Central Organizing Hub**: A specific set of genes, termed the Critical Point (CP), exhibits bimodal singular behavior based on the *nrmsf* metric. The CP functions as a central hub, spreading high variability and driving critical transitions. When the system deviates from homeostasis, changes at the CP propagate perturbations throughout the genome, demonstrating SOC in genomic regulation [Tsuchiya et al., 2023a].
3. **Modeling the Genome Engine as a Dynamical System**
   The genome engine can be modeled as a one-dimensional dynamical system [Tsuchiya et al., 2023b]. The CM's expression level at time ε_t represents "position," its first difference ($\varepsilon_{t+1} - \varepsilon_t$) represents "momentum," and its second difference ($\varepsilon_{t+1} - 2\varepsilon_t + \varepsilon_{t-1}$) acts as an "effective force" influencing energy changes. This framework, grounded in stochastic thermodynamics [Parrondo et al., 2015; Ito, 2018; Peliti and Pigolotti, 2021;

Shiraishi, 2023; Korbel and Wolpert, 2024], illustrates how the genome maintains a near balance of influx and outflux while dynamically interacting with its environment.

4. **Transition-Driven Switching of Cyclic Flows**: Critical transitions in the genome engine reverse cyclic expression fluxes [Tsuchiya et al., 2020, 2022]. These transitions are linked to structural changes, such as the bursting of peri-centromeric domains (PADs) in MCF-7 cancer cells, which affect chromatin folding and enable dynamic genomic regulation [Zimatore et al., 2021; Krigerts et al., 2021; Erenpreisa et al 2023].
5. **OMG–CP–GA Network Synchronizing CP and GA for Cell-Fate Change**: The OMG–CP–GA network governs cell-fate transitions by coordinating interactions among Oscillating-Mode Genes (OMG), the CP, and the GA. OMGs, identified by high scores on the second principal component (PC2) [Zimatore et al., 2021], modulate synchronization between the CP and GA. This synchronization maintains genome-wide balance and triggers critical transitions, leading to coordinated shifts in genome expression and chromatin remodeling [Tsuchiya et al., 2023a].
6. **Advancements over Classical Self-Organized Criticality Models**: Unlike classical SOC (cSOC) models, which involve state transitions from subcritical to supercritical toward a critical attractor [Bak et al., 1987, 1988; Bak and Chen, 1991; Watkins et al. 2016], our SOC model features a dynamic CP that actively induces state changes to guide cell-fate transitions. This mechanism enables the genome to adaptively regulate itself in response to stimuli [Tsuchiya et al., 2016, 2020, 2022].
7. **A Universality Across Biological Systems:** The SOC control of genome expression is demonstrated in distinct biological systems, including cell differentiation and embryonic development: HRG- and EGF-stimulated MCF-7 cells [Saeki et al., 2009], atRA- and DMSO-stimulated HL-60 cells [Huang et al., 2005], Th17 cell differentiation [Ciofani et al., 2012], and early embryonic development in mice [Deng et al. 2014] and humans [Yang et al., 2013]. These findings highlight the robustness and universality of the dynamic criticality model [Giuliani et al., 2017; Tsuchiya et al., 2016, 2020, 2022].

Building on these findings and utilizing our dynamical approach, this study aims to elucidate how non-equilibrium thermodynamic principles regulate genome expression, distinguish between effective and non-effective dynamics in cell-fate change, and investigate a unified framework for integrating expression flux analysis with genomic thermodynamics.

We analyze temporal gene expression data from MCF-7 cancer cell lines stimulated with Epidermal Growth Factor (EGF), which promotes proliferation without altering cell fate, and Heregulin (HRG), which commits cells after a relatively rapid decay of the gene expression perturbation to differentiate [Saeki et al., 2009; Zimatore et al., 2021; Erenpreisa et al., 2023]. By modeling these two processes as open stochastic thermodynamic systems, characterized by exchanges of heat and matter (e.g., gases, nutrients, and wastes) with their surroundings and also by inherent randomness, we capture the dynamic and non-deterministic nature of genome regulation influenced by both external and internal factors.

To assess differences in genome expression dynamics, we use Shannon entropy and mutual information as measures of disorder and predictability. Shannon entropy, rooted in information theory, quantifies unpredictability in biological processes and relates to entropy production in nonequilibrium systems, linking informational disorder to energy dissipation. This framework explains how biological systems maintain order and perform work under stochastic, far-from-equilibrium conditions. Mutual information, on the other hand, captures interdependencies within the gene expression system, revealing regulatory relationships in a quantitative manner.

Within the framework of stochastic thermodynamics, mutual information is essential for understanding feedback, control mechanisms, thermodynamic efficiency, and information flow [Shannon, 1948; Adami, 2004; Hübner and Szekely, 2010; Sagawa and Ueda, 2012a, 2012b; Barato and Seifert, 2014]. A key historical perspective on the interplay between information and thermodynamics comes from Maxwell's demon, a thought experiment introduced by physicist James Clerk Maxwell [Maxwell, 1871].

Maxwell's demon sorts molecules to reduce entropy in a closed system, seemingly violating the second law of thermodynamics. However, extensive studies [Szilárd, 1929; Landauer, 1961; Astumian, 1997; Bennett, 2003; Toyabe et al., 2010; Bérut et al., 2012; Sagawa and Ueda, 2012a, 2012b; Seifert, 2012; Flatt et al., 2023; Annby-Andersson et al., 2024] have demonstrated that Maxwell's demon is not merely a paradox but a key concept for understanding the relationship between information and thermodynamics. These studies show that the demon's ability to measure, store, and process information incurs a thermodynamic cost, thereby preserving the second law. Far from being just a metaphor, Maxwell's demon embodies a functional principle, validated through experimental systems and biological processes, underscoring the profound connection between information processing and thermodynamic behavior in non-equilibrium systems, including the phenomena of life.

The overview and objectives of our study are as follows:

Understanding complex gene expression networks requires accurate estimation of information-theoretic metrics such as Shannon entropy and mutual information, which quantify disorder, predictability, and interdependencies. These metrics are challenging to estimate due to the stochastic nature of gene expression and the complexity of underlying networks.

To address this, we employ Coherent Stochastic Behavior (CSB) through a convergence-based approach [Tsuchiya et al., 2014, 2015, 2016]. This enhances the estimation of the CP (Critical Point) location along *nrmsf* (**section 2.1**) and ensures robust identification of CP genes by grouping them based on their expression variability (**section 2.2**). Additionally, this approach improves the robustness of thermodynamic metrics, including entropy and mutual information, which quantify the dynamics of genomic regulation (**section 2.3**). This methodology allows us to characterize the genomic mechanisms underlying stimuli that do not promote cell-fate change (EGF stimulation) versus those that drive cell-fate transitions (HRG stimulation).

Our study focuses on the following objectives:

1. **Open Thermodynamic Modeling and Phase Synchronization** (**section 2.4**): We develop a data-driven approach to model an open stochastic thermodynamic system of MCF-7 cell lines and investigate how order-disorder phase synchronization between the CP and the Whole Expression System (WES) regulates genome expression under EGF and HRG stimulation.
2. **High-Order Mutual Information** (**section 2.4**): We investigate complex nonlinear interdependencies in networks within the WES by identifying high-order mutual information.
3. **CP as Maxwell's Demon-Like Rewritable Chromatin Memory** (**sections 2.5** and **2.6**): We examine the CP's role as a Maxwell's demon-like rewritable chromatin memory, clarifying its function in entropy regulation and information flow, thereby deepening our understanding of genomic thermodynamics.

In the Discussion, we address how an order parameter for phase synchronization emerges, unifying expression flux analysis with genomic thermodynamics. These findings pave the way for leveraging genome intelligence (GI) through autonomous genome computing, offering new

strategies for controlling cell fate and developing cancer therapies. Finally, the key insights are summarized in the Conclusion.

2. Results

2.1 A Metric Parameter for Self-Organization of Whole-Genome Expression

To identify the Critical Point (CP) genes, which exhibit critical behavior, we introduce a metric parameter that quantifies the self-organization of time-series whole-genome expression data obtained from both microarray and RNA-Seq datasets (see methodological details in [Tsuchiya et al. 2023b]. This metric parameter is defined by the root mean square fluctuation ($rmsf_i$), representing the standard deviation of a gene's expression levels over time, calculated as follows:

$$rmsf_i = \sqrt{\frac{1}{T}\sum_{j=1}^{T}\left(\varepsilon_i(t_j) - \langle\varepsilon_i\rangle\right)^2}, \quad (1)$$

where $\varepsilon_i(t_j)$ is the expression level of the ith gene at a specific cell state or experimental time point t_j, $\langle\varepsilon_i\rangle$ is the average expression level of the ith gene over all time points, T is the total number of cell states or experimental time points.

To compare gene expression variability across different biological systems [Tsuchiya et al., 2020, 2022], we normalize the $rmsf_i$ value by the maximum *rmsf* observed in the dataset, resulting in the normalized *rmsf* ($nrmsf_i$). For each gene expression value measured across experimental time points, we first compute $nrmsf_i$ and then take its natural logarithm; in our study, "expression" specifically refers to this logarithm. This transformation captures scaling response behaviors in SOC control [Tsuchiya et al., 2015, 2016, 2023b; Giuliani et al., 2017] and noise reduction.

For microarray data, which rarely contain zeros, this approach works effectively. In contrast, RNA-Seq data, often characterized by numerous zero values, require adding a small random noise to zeros, performing ensemble averaging, and then applying the logarithmic transformation to preserve coherent stochastic behavior (CSB) [Tsuchiya et al., 2023b].

The selection of $nrmsf_i$ as the ranking parameter is biologically motivated. Gene expression variability serves as a proxy for chromatin flexibility, where higher variability reflects increased chromatin accessibility and dynamic regulation. Supporting this, a recent study on MCF-7 cell fate changes used Principal Component Analysis (PCA) of genome expression profiles to show that $nrmsf_i$ values align with the underlying chromatin's structural flexibility [Zimatore et al., 2021]. Furthermore, experimental findings [Krigerts et al., 2021; Erenpreisa et al., 2023] have demonstrated that chromatin remodeling is pivotal for the SOC control of genome expression, where CP genes act as regulatory hubs that orchestrate genome-wide transitions.

2.2 Identifying CP Genes Using the Metric Parameter

The whole-genome mRNA expression dataset is analyzed using *nrmsf* as the metric parameter. Genes are first sorted in descending order of *nrmsf* and then grouped into clusters large enough to capture genome-wide averaging behavior of collective expression dynamics [Tsuchiya et al., 2014, 2015, 2016]. Coherent Stochastic Behavior (CSB) in gene expression emerges when the sample size (n) exceeds 50 [Censi et al., 2011]. As the sample size increases, the group's center of mass (CM) with unit mass converges to a constant value, driven by the law of large numbers. This convergence reflects a nearly balanced inflow and outflow of expression flux within the Whole Expression System (WES) [Tsuchiya et al., 2023b] (see more in **section 2.4**). To grasp such types of thermodynamic behavior, each group is needed to contain more than 200 genes.

In **Figure 1**, the Critical Point (CP) region is identified through temporal changes in overall expression along the *nrmsf* metric. The CP region demonstrates distinct bimodal singluar behavior, separating high-variance (super-critical) and low-variance (sub-critical) states. In **Figure 2**, the convergence of randomly selected gene expressions in critical states (CSB) to the center of mass (CM) of the critical state enables the identification of these distinct response domains.

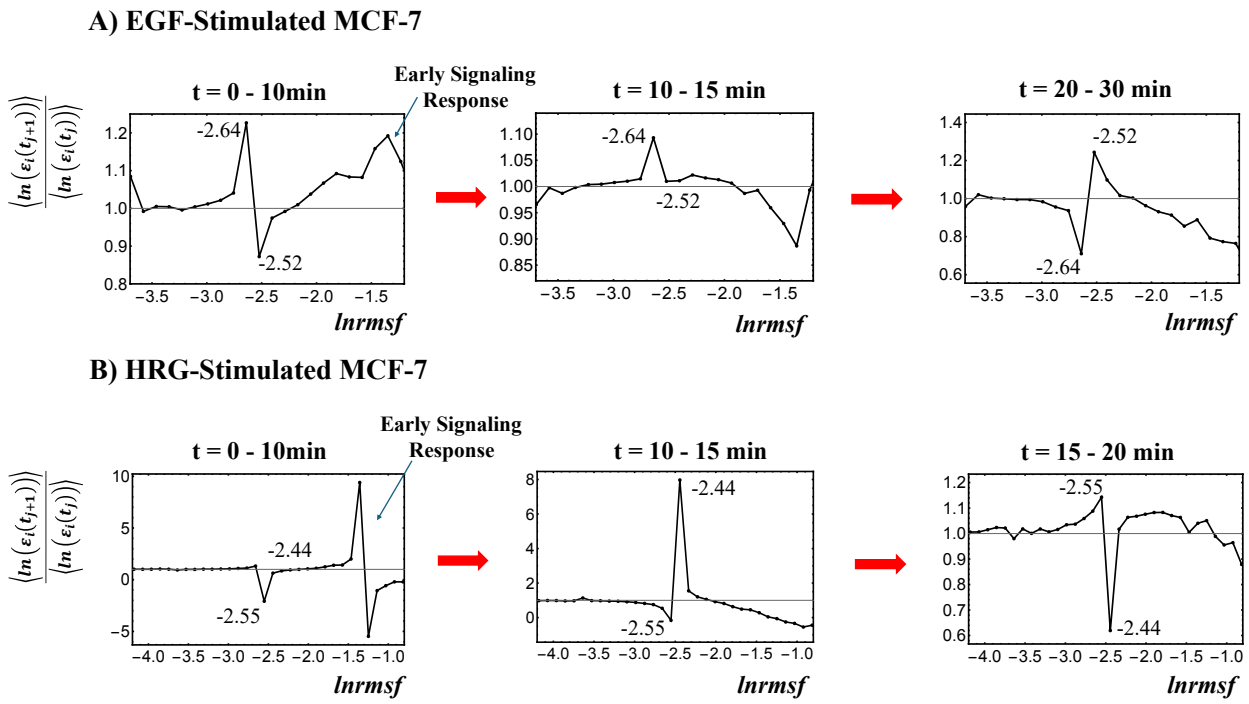

Figure 1: Identification of the Critical Point (CP) Region with Distinct Response Domains. A) EGF-stimulated MCF-7 cells and B) HRG-stimulated MCF-7 cells. According to the *nrmsf* metric parameter, whole expressions are sorted and grouped into 40 equal *nrmsf* ranges, excluding groups with fewer than 200 genes, which typically occur in the highest and lowest regions. The *x*-axis represents the natural logarithm of the average *nrmsf* value, $<nrmsf_i>$ for the ith group, denoted by a black solid dot, while the *y*-axis represents the temporal expression response, calculated as the ratio of the group expression average between consecutive time points, $<ln(\varepsilon_i(t_{j+1}))>/<ln(\varepsilon_i(t_j))>$. Under EGF: **A**) stimulation, CP genes exhibit bimodal critical behavior with peaks ranging from -2.64 to -2.52 *ln*(*nrmsf*), while under HRG: **B**) stimulation, the peaks range from -2.55 to -2.44 *ln*(*nrmsf*). The CP region effectively separates high-variance (super-critical) and low-variance (sub-critical) responses, highlighting distinct regulatory domains within the genome. Notably, the CP region includes not only the CP genes themselves but also the surrounding edge genes, further demonstrating its extensive influence.

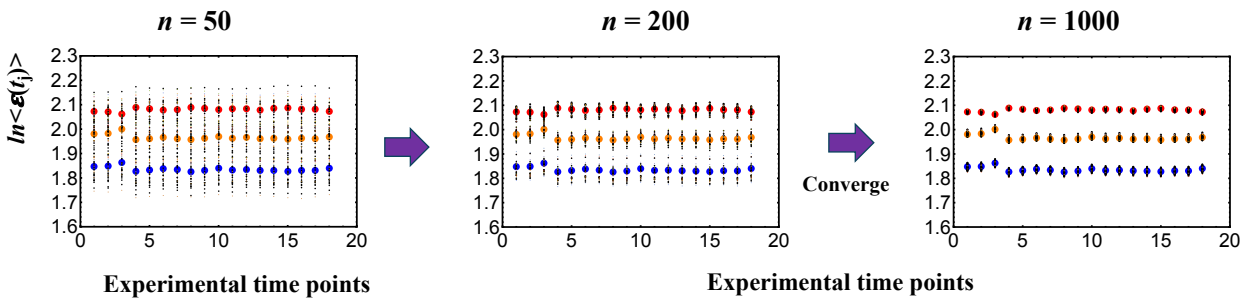

Figure 2: Utilization of Coherent Stochastic Behaviors (CSBs) for Critical-State Attractors. Bootstrapping analysis demonstrates the convergence of the center of mass (CM) of randomly selected gene expressions (sample sizes of n = 50, 200,1000) from critical states. For each random sampling, 40 repetitions are performed across experimental time points, depicted by small dots. This convergence highlights the CM of a critical state acting as an attractor. The large colored dots represent the CM of critical states: red indicates the super-critical state, orange denotes CP-region genes, and blue signifies the sub-critical state. The numbers of gene expressions for the super-critical, sub-critical, and CP-region genes are 10514, 7917, and 3846 (**Figure 1**), respectively. The x-axis corresponds to experimental time points (see Material) and the y-axis represents the natural logarithm of the average group expression.

2.3 Open Stochastic Thermodynamic Model of MCF-7 Cell Lines

This section presents a stochastic thermodynamic model of MCF-7 breast cancer cell lines, focusing on the interaction between the critical point (CP) gene region and the rest of the whole gene expression system (WES). The remaining genes in WES are collectively referred to as the Peripheral Expression System (PES).

We adopt an open thermodynamic framework in which cells continuously exchange heat and substances (gases, nutrients, and wastes) with their environment. This exchange influences gene expression dynamics. By analyzing temporal entropy variations within the system, we gain insights into how entropy constrains the organization and stability of genomic regulation. This approach highlights open thermodynamic principles that govern these genomic-level interactions.

As illustrated in Figure 3, both the CP genes and the PES exchange energy with the external environment (OUT). We analyze an ensemble of CP genes and the PES within the cancer cell population, examining their entropy and interactions to uncover the open thermodynamic properties governing the system.

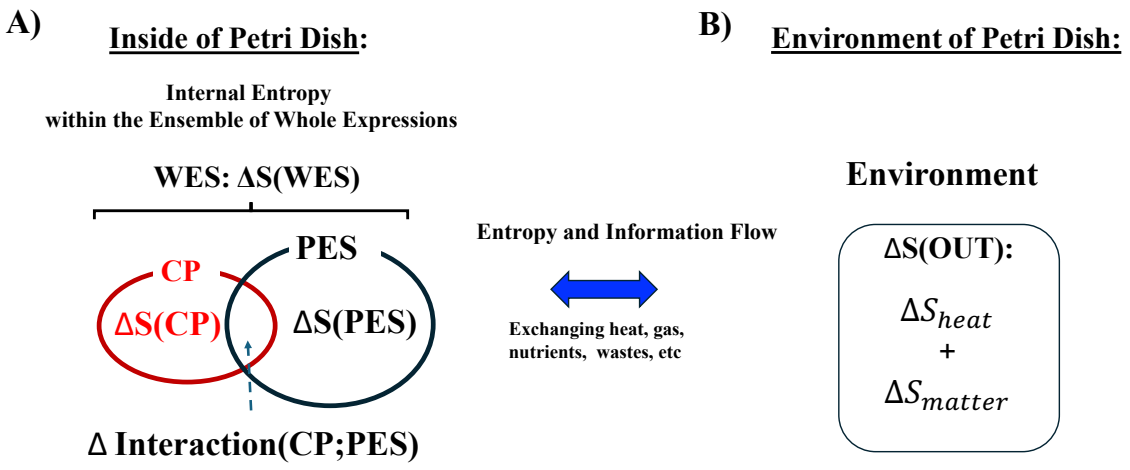

Figure 3: Open Stochastic Thermodynamic Model Setup for MCF-7 Cell Lines.

This schematic depicts an open thermodynamic system for MCF-7 cell lines, where heat, gases, nutrients, and wastes are continuously exchanged with the environment. The system includes the Whole Expression System (WES), which comprises both a set of Critical Point (CP) genes and the remaining genes, referred to as the Peripheral Expression System (PES). Each component has its own entropy: S(WES), S(CP), and S(PES).

A) The total entropy change of WES (ΔS(WES)) is decomposed into changes in CP (ΔS(CP)), PES (ΔS(PES)), and their interaction term (ΔInteraction(CP;PES)). This decomposition enables investigation of how these interaction terms relate to the mutual information ΔI(CP;PES).

B) Entropy exchange with the environment (ΔS(OUT)) is further broken down into contributions from heat (ΔS(heat)) and material exchange (ΔS(matter)).

We apply the Coherent Stochastic Behavior (CSB) method to estimate entropy and mutual information, demonstrating consistent convergence behavior despite the inherent randomness of individual genes (see **Figure 4**).

A) EGF-MCF-7 Cells

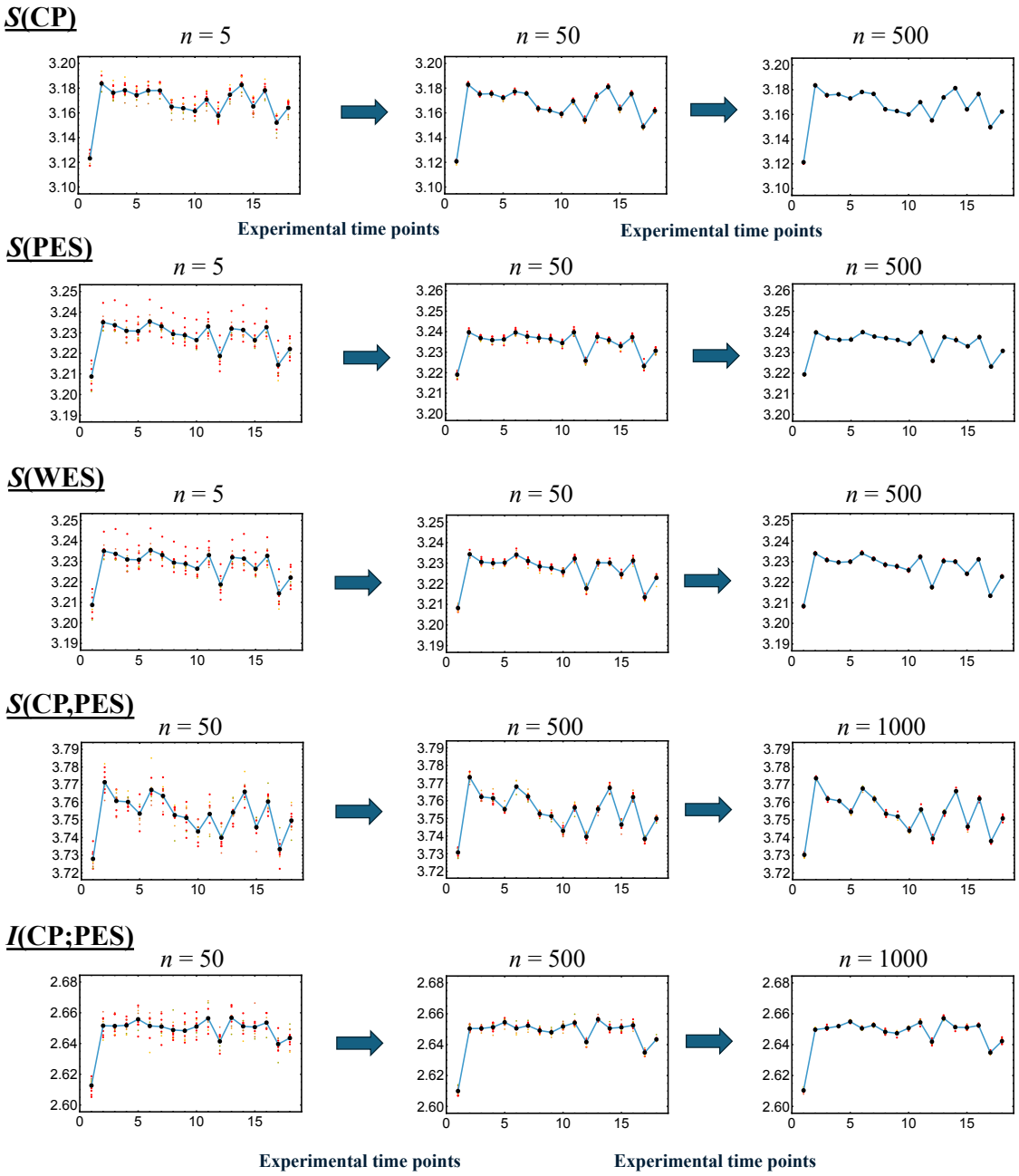

B) HRG-MCF-7 Cells

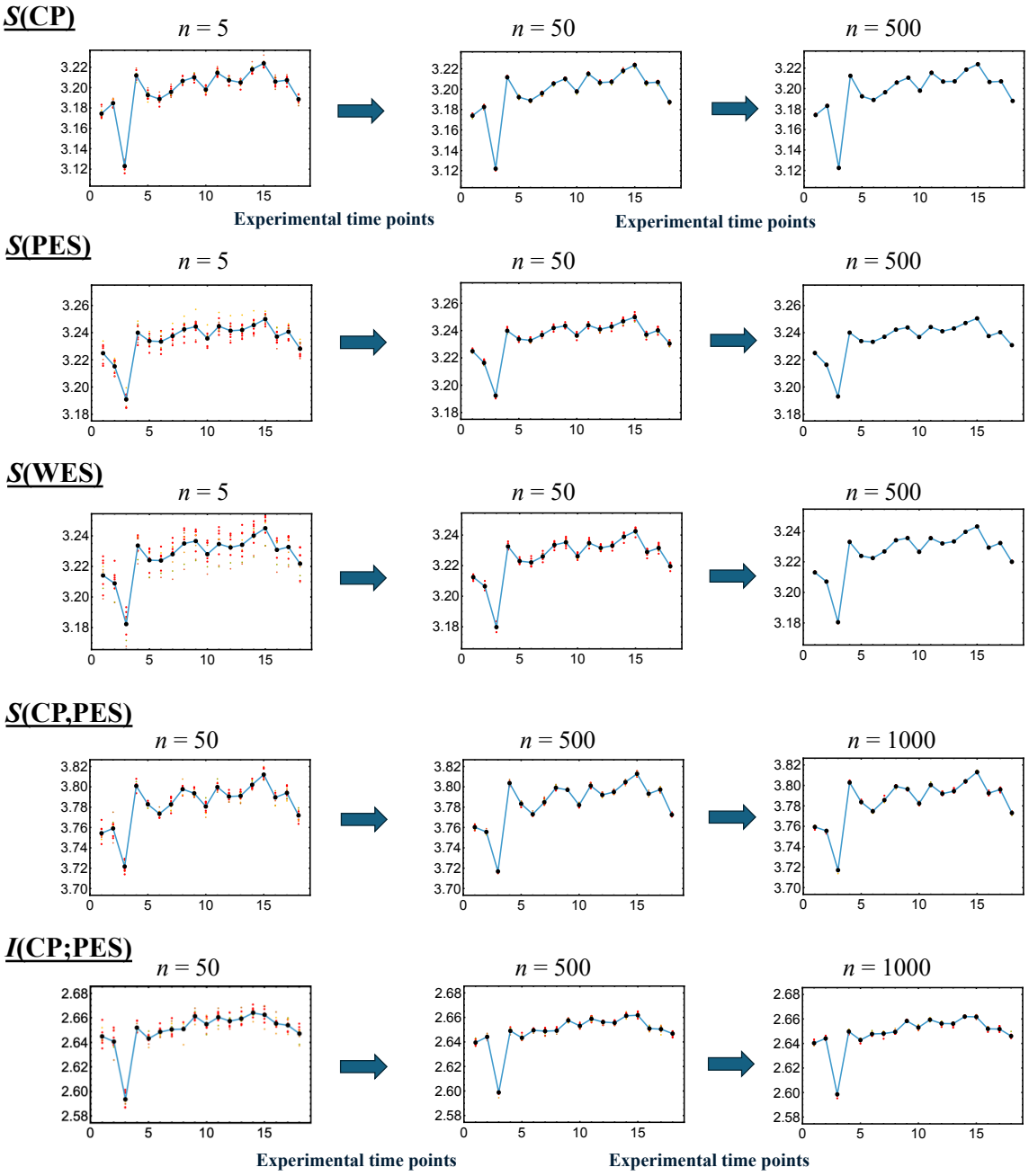

Figure 4: Convergence-based Approach for Robust Estimation of Information-Thermodynamic Metrics. **A)** EGF-stimulated and **B)** HRG-stimulated MCF-7 cells. This figure illustrates the convergence of various information-thermodynamic metrics in HRG-stimulated MCF-7 cancer cells: the entropies of the critical point (S(CP)), whole expression system (*S*(WES)), and peripheral expression system (S(PES)); the joint entropy (*S*(CP, PES)); and the mutual information (*I*(CP; PES)). These metrics were computed using a bootstrapping analysis with a fixed sample size of 1000 and a bin size of 30 and increasing numbers of repetitions, (n = 5, 50, 200) for entropy and (n = 50, 500, 1000) for mutual information and joint entropy, to assess convergence. Small red solid circles represent

fluctuations in the average values obtained from each of the 10 bootstrapping iterations, while the large black circles indicate the overall average value across all 10 repetitions. Mutual information and joint entropy converge more slowly than entropy because they require evaluating a two-dimensional joint frequency table rather than a one-dimensional one. On the *x*-axis, experimental time points are plotted, while the *y*-axis shows the values of the respective information-thermodynamic metrics. The detailed procedure is illustrated in the Figure in section 2.6.

In **Figure 2**, increasing the number of genes sampled demonstrates the convergence of the center of mass (CM) of gene expressions, highlighting the attractor behavior of critical states. In contrast, **Figure 4** illustrates that with a fixed sample size (30), increasing the number of sampling repetitions through bootstrapping yields a robust estimation of information thermodynamic metrics. This approach leverages CSB to achieve the convergence of average values across samplings, thereby stabilizing these estimates and elucidating the thermodynamic principles underlying the genome's dynamic regulatory mechanisms. Additionally, the second thermodynamic condition is considered, accounting for entropy flow between the cell line and its external environment (beyond the confinement of the Petri dish), as described below.

1): **Random Sampling**: We repeatedly random sample of genes from the CP, PES and WES datasets, allowing for replacement (bootstrap sampling).

2): **Calculating Entropy**: For each sample, we calculate the Shannon entropy using the following equation:

$$S\left(X\left(t_j\right)\right) = -\sum_i P\left(x_i\left(t_j\right)\right) ln\left(P\left(x_i\left(t_j\right)\right)\right) \quad (2)$$

where $S(X(t_j))$ is dimensionless; $X(t_j)$ represents CP(t_j), PES(t_j) or WES(t_j) and $P(x_i(t_j))$ is the probability of gene x_i being expressed at t_j.

Note that regarding **Figure 4**, we observed that varying the bin sizes used to calculate the probability distributions leads to consistent offsets in the resulting information-thermodynamic metrics (e.g., entropy), with larger bin sizes producing higher values. This behavior is exactly as expected for entropy as a proper state function. We chose a bin size of 30 for the probability distributions, following the Square Root Rule (bin size ~ $\sqrt{n}$, where n is the sample size), as described in [Tsuchiya et al., 2010].

3): **Relating Entropies and High-Order Mutual Information**: We compute the joint entropy S(CP, PES) at t_j:

$$S\left(CP(t_j), PES(t_j)\right) = -\sum_{x_{i\in CP}, y_j \in PES} P\left(x_i(t_j), y_j(t_j)\right) ln\left(P\left(x_i(t_j), y_j(t_j)\right)\right) \quad (3)$$

where $P(x_i(t_j), y_j(t_j))$ is the joint probability of CP gene x_i and and PES gene y_j being simultaneously expressed at t_j. To estimate the joint probability distribution between CP and PES genes, we construct a two-dimensional joint frequency table at each time point using a bootstrapping approach and a fixed bin size of 30.

The mutual information (MI) between CP and PES, I(CP: PES) is given by

$$I\left(CP(t_j); PES(t_j)\right) = S\left(CP(t_j)\right) + S\left(PES(t_j)\right) - S\left(CP(t_j), PES(t_j)\right). \quad (4)$$

The joint entropy S(CP, PES) can also be expressed as internal entropy:

$$S_{internal} = S\left(CP(t_j), PES(t_j)\right) = S\left(CP(t_j)\right) + S\left(PES(t_j)\right) - I\left(CP(t_j); PES(t_j)\right), \quad (5)$$

where the mutual information is subtracted to remove shared information, leaving only the unique and combined uncertainties of the two components. From this point onward, the time t_j will be omitted for simplicity, except when explicitly necessary.

Note that WES consists of CP genes and the remaining WES genes (PES). The entropies S(WES), S(CP), and S(PES) are calculated from their respective gene sets using the same bootstrap procedure and a dimensionless entropy measure, accounting for interactions with the external environment (**Figure 3**). As shown in **Figure 5**, S(WES) differs from $S_{internal}$ (equation (5)) at all time points, indicating that the standard mutual information formula (equation (4)) does not fully capture all dependencies in MCF-7 cancer cells:

$$S(WES) \neq S_{internal} = S(CP, PES). \quad (6)$$

By replacing S(CP,PES) in eqaution (4) with S(WES), the net MI including high-order terms, I_{net}(CP; PES) is defined as:

$$I_{net}(CP; PES) = \{S(CP) + S(PES)\} - S(WES). \quad (7)$$

Therefore, from equations (4) and (7), the high-order MI, I_{high}(CP; PES) can be defined and observed as postive for the entire experimental time:

$$\begin{aligned} I_{high}(CP; PES) &= I_{net}(CP; PES) - I(CP; PES) \\ &= \{S(CP) + S(PES)\} - S(WES) - \{S(CP) + S(PES) - S(CP; PES)\} \\ &= S(CP; PES) - S(WES) > 0 \end{aligned} \quad (8)$$

High-order mutual information (MI) [McGill, 1954; Hu, 1962; Timme et al., 2014; Rosas et al., 2019] extends beyond standard MI by capturing collective and network-level effects, including overlapping gene functions, feedback loops, and nonlinear interdependencies that simple pairwise correlations cannot fully explain. **In Figure 5**, a positive high-order MI (I_{high} >0) under both EGF and HRG stimulation indicates that the total system entropy S(WES) is less than the combined CP and PES entropies. This suggests the presence of redundancy (overlapping information) and synergy (collective effects exceeding pairwise contributions) in the MCF-7 genomic network; see partial information decomposition [Williams and Randall, 2010]. These findings support the presence of backup mechanisms, overlapping functions (redundancy), and emergent collective regulation (synergy) in a typical biological genomic network.

In **Figure 6**, under both EGF and HRG stimulations, the net MI, I_{net}(CP; PES)) are nearly equivalent to the CP entropy S(CP):

$$I_{net}(CP; PES) \sim S(CP) + 0.007 \text{ for EGF stimulation} \quad (9)$$

and

$$I_{net}(CP; PES) \sim S(CP) + 0.010 \text{ for HRG stimulation.} \quad (10)$$

Since the net MI exceeds S(CP) slightly, it reflects the positive high-order MI contribution. This result clearly demonstrates that CP genes drive coordinated transitions between ordered and disordered phases between CP and PES. Moreover, it provides a thermodynamic framework to explain how state changes in the CP can drive large-scale 'genome avalanches,' as demonstrated through expression flux analysis [Tsuchiya et al., 2023a].

4): **Second Law of Thermodynamics:** In our open system, the whole expression system comprising CP genes and PES, the entropy production (σ) quantifies the irreversible processes occurring within the system. Compliance with the second law of thermodynamics mandates that entropy production must be non-negative ($\sigma \geq 0$), representing the irreversibility inherent in processes like metabolic reactions, molecular interactions, and active transport mechanisms. Dimensionless entropy production (σ) is mathematically defined as the difference between the total change in the WES entropy ($\Delta S(WES)$) and the entropy flow exchanged with the external environment of the culture medium ($\Delta S(OUT)$):

$$\sigma = \Delta S(WES) - \Delta S(OUT) \geq 0 \,. \tag{11}$$

The change in entropy of the outside environment, $\Delta S(OUT)$ is given by

$$\Delta S(OUT) = \Delta S_{heat} + \Delta S_{matter}, \tag{12}$$

where

$$\Delta S_{heat} = \frac{Q}{T} \tag{13}$$

represents the entropy change due to heat (Q) exchange at a temperature (T = 37 °C), and ΔS_{matter} is the net entropy exchange associated with the inflow and outflow of substances:

$$\Delta S_{matter} = \sum_{out} n_{out} \cdot s_{out} - \sum_{in} n_{in} \cdot s_{in}, \tag{14}$$

where n_{in} and s_{in} represent the molar quantity and molar entropy of inflowing substances, and n_{out} and s_{out} for outflows.

Cells generate heat through metabolic activities (e.g., ATP synthesis, substrate oxidation), exchange nutrients (e.g., glucose, amino acids) and waste products (e.g., CO_2, lactate) with the environment.

Therefore, we obtain the second law condition for the system:

$$\sigma = \Delta S(WES) - \left(\frac{Q}{T} + \Delta S_{matter}\right) \geq 0. \tag{15}$$

Internal entropy production σ must be non-negative ($\sigma \geq 0$) to satisfy the second law of thermodynamics. This ensures that all irreversible processes within the cell culture contribute to an overall increase in entropy.

2.4 Genomic-Thermodynamic Phase Synchronization Between CP Genes and the Whole Expression System

The genomic-thermodynamic phase synchronization for EGF-stimulated and HRG-stimulated MCF-7 cells is summarized below:

EGF-stimulated MCF-7 cells (non-cell fate change): EGFR activation drives entropy changes in CP and PES genes within the first 10 minutes. Afterward, information-thermodynamic metrics fluctuate around average values through synchronized order-disorder phases, guided by net mutual information dynamics scaling with CP entropy. WES maintains a dynamic balance of entropy and information flux.

HRG-stimulated MCF-7 cells (cell fate change): PES exhibits stronger phase synchronization with CP than under EGF stimulation via net mutual information dynamics. A critical transition at 10-30 minutes activates the CP as a Maxwell demon, driving feedback to PES and genomic avalanche. This leads to a pulse-like perturbation in all information-thermodynamic metrics.

A key difference between EGF and HRG stimulation is the emergence of a critical transition through the activation of the Maxwell demon (**sections 2.5** and **2.6**).

Further details are provided below:

1) In EGF-stimulated MCF-7 cells:

A) Dissipative Thermodynamic Synchronization of Order-Disorder Phases

In EGF-stimulated MCF-7 cells, EGFR activation triggers the MAPK/ERK pathway for gene regulation and the PI3K/AKT pathway for survival, driving proliferation within the first 10 minutes [Saeki et al., 2009]. This activation induces marked changes

in the entropy of the CP region genes and PES, as evidenced by the rise in net mutual information, I_{net}(CP;PES)), during the initial 0–10 minutes (**Figure 5A**).

The increase in I_{net}(CP;PES) reflects nonlinear interactions between CP and PES that expand both of their accessible state microspaces, such as different gene expression patterns, protein states, or regulatory interactions, which indicates active exchanges of heat and matter with the environment. As CP's complexity grows, its nonlinear influence on PES strengthens, promoting greater integration between these subsystems. Furthermore, the phase synchronization between CP and PES, characterized by coordinated shifts between ordered and disordered phases (**Figure 6A**), yields a high Pearson correlation (r = 0.90). This synchronization is fundamentally driven by I_{net}(CP;PES), which combines standard mutual information with positive higher-order MI (**section 2.3**) and scales with S(CP).

B) Dynamic Equilibrium Underpinning Coherent Stochastic Behavior (CSB)

In **Figure 5A**, the whole expression system's entropy, S(WES), fluctuates only slightly around an average of 3.17 (within $\pm 6.22\times10^{-2}$), indicating that large-scale homeostasis can coexist with continuous environmental exchanges. This balance of entropy and information flux preserves overall stability and supports coherent stochastic behavior (CSB). The observation aligns with expression flux analyses [Tsuchiya et al., 2020, 2023a], suggesting a biophysical basis for the law of large numbers, where collective system behavior remains stable despite the inherent stochasticity of individual molecular interactions.

2) In HRG-stimulated MCF-7 cells:

Activation of the CP as a Maxwell Demon

In contrast to the large initial disorder changes induced by EGF in the first 0–10 minutes, HRG stimulation triggers pulse-like order-disorder transitions in all information-thermodynamic metrics, including both S(CP) and S(PES) as net mutual information I_{net}(CP;PES) rises during the 10–20 minute period (**Figure 5B**). This suggests more active exchanges of heat and matter with the environment under HRG, strengthening phase synchronization. The pulse-like critical transition aligns with findings from PCA analysis [Zimatore et al., 2021] and expression flux analysis [Tsuchiya et al., 2020, 2022]. It involves the CP acting as a Maxwell demon (see detailed analysis in later

sections), inducing feedback to the PES and orchestrating a genomic avalanche that drives cell-fate change.

From a biological standpoint, compared to EGF stimulation, HRG stimulation activates the ERK/Akt pathway within 5-10 minutes, leading to a ligand-specific, biphasic induction of AP-1 complex components (e.g., c-FOS, c-JUN, FRA-1) and the transcription factor c-MYC [Nagashima et al., 2007; Saeki et al., 2009; Nakakuki et al., 2010].

By 15-20 minutes, this cascade produces a pulse-like, genome-wide perturbation marked by the activation of oscillating-mode genes (OMGs), as shown by expression flux analysis [Tsuchiya et al., 2023a]. These genes emit large expression fluxes to both the CP and the genome attractor (GA), facilitating their synchronization within the OMG–CP–GA network.

At 60 minutes, this critical transition is followed by a peak in c-MYC expression [Krigerts et al., 2021; Erenpreisa et al., 2023], resulting in extensive gene amplification. Beyond this point, entropy changes exhibit steady fluctuations with damping behavior, as also observed in both PCA and expression flux analyses. This indicates balanced large-scale energy flows that sustain cellular homeostasis.

These findings on EGF- and HRG-stimulations demonstrate that changes in entropy and net mutual information effectively serve as indicators of fundamental cellular processes, including the activation of signaling pathways, occurrence of critical transitions, and synchronization of genome expression. Adopting this thermodynamic perspective enriches our understanding of how different stimuli orchestrate complex regulatory networks within cells.

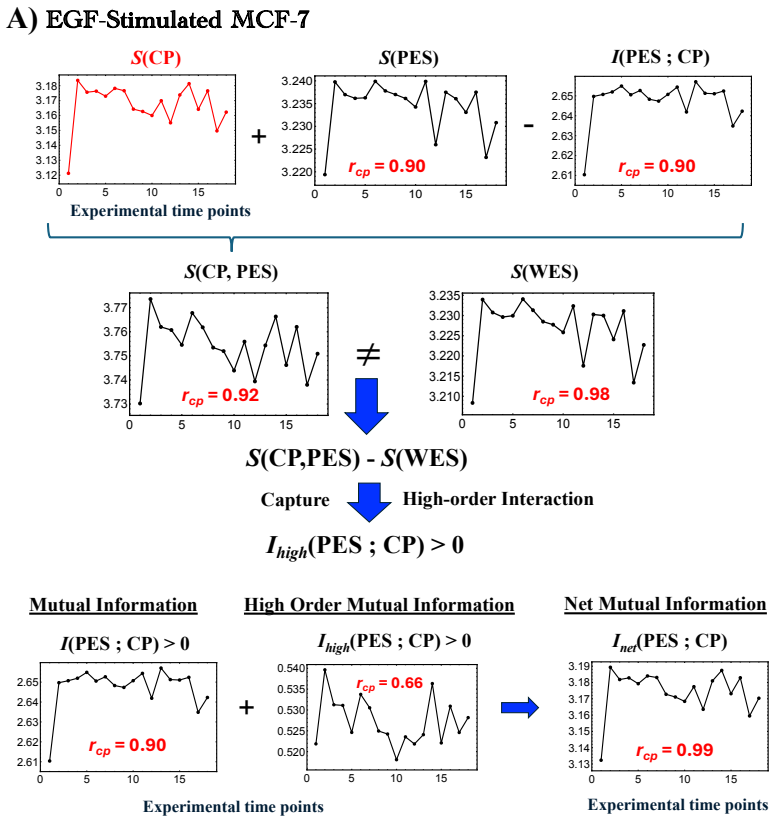
A) EGF-Stimulated MCF-7
S(CP)
S(PES)
I(PES ; CP)
r_cp = 0.90
r_cp = 0.90
Experimental time points
S(CP, PES)
S(WES)
r_cp = 0.92
r_cp = 0.98
S(CP,PES) - S(WES)
Capture
High-order Interaction
I_high(PES ; CP) > 0
Mutual Information
High Order Mutual Information
Net Mutual Information
I(PES ; CP) > 0
I_high(PES ; CP) > 0
I_net(PES ; CP)
r_cp = 0.90
r_cp = 0.66
r_cp = 0.99
Experimental time points
Experimental time points

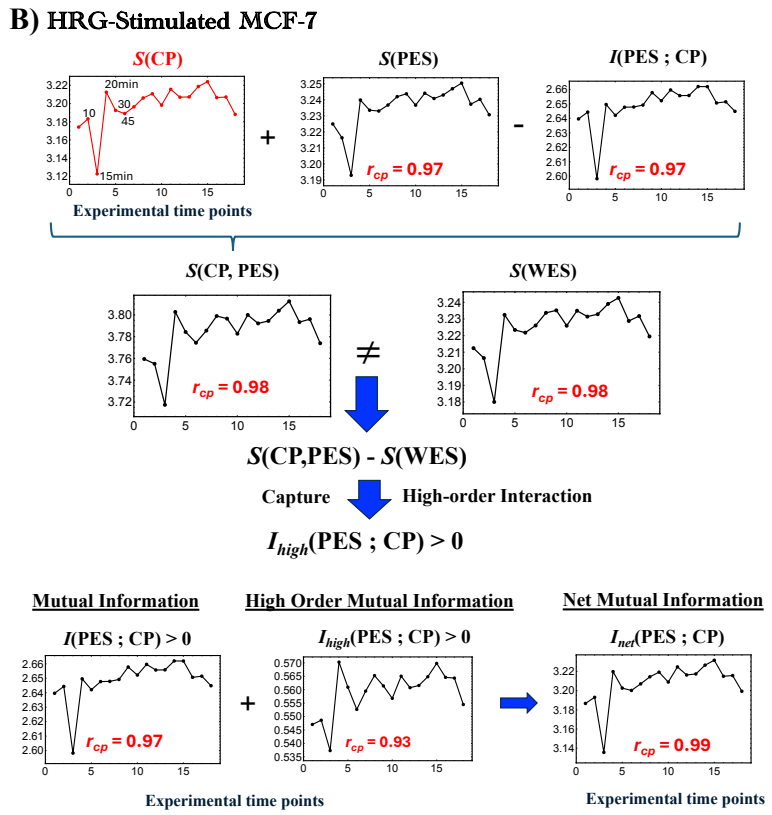
B) HRG-Stimulated MCF-7
S(CP)
S(PES)
I(PES ; CP)
20min
10
30
45
15min
r_cp = 0.97
r_cp = 0.97
Experimental time points
S(CP, PES)
S(WES)
r_cp = 0.98
r_cp = 0.98
S(CP,PES) - S(WES)
Capture
High-order Interaction
I_high(PES ; CP) > 0
Mutual Information
High Order Mutual Information
Net Mutual Information
I(PES ; CP) > 0
I_high(PES ; CP) > 0
I_net(PES ; CP)
r_cp = 0.97
r_cp = 0.93
r_cp = 0.99
Experimental time points
Experimental time points

Figure 5. Thermodynamic Phase Synchronization and Higher-Order Mutual Information in MCF-7 Cells. A) EGF-stimulation and **B)** HRG-stimulation. We adapt the bootstrapping results of average values, using 500 repetitions for entropy and 1000 repetitions for mutual information and joint entropy (**Figure 4**) to estamate high-order mutual information. For both EGF and HRG stimulations, the difference between *S*(WES) and *S*(CP, PES) reveals positive higher-order mutual information, denoted as I_{high}(CP; PES). The net mutual information, I_{net}(CP; PES), which encompasses both standard mutual information and higher-order mutual information, scales with S(CP). The *y*-axis represents the measured values, while the *x*-axis shows time points at 0, 10, 15, 20, 30, 45, 60, 90, 120, 180, 240, 360, 480, 720, 1,440, 2,160, 2,880, and 4,320 minutes. For further details, refer to the main text.

A) Phase synchronization: EGF-stimulation

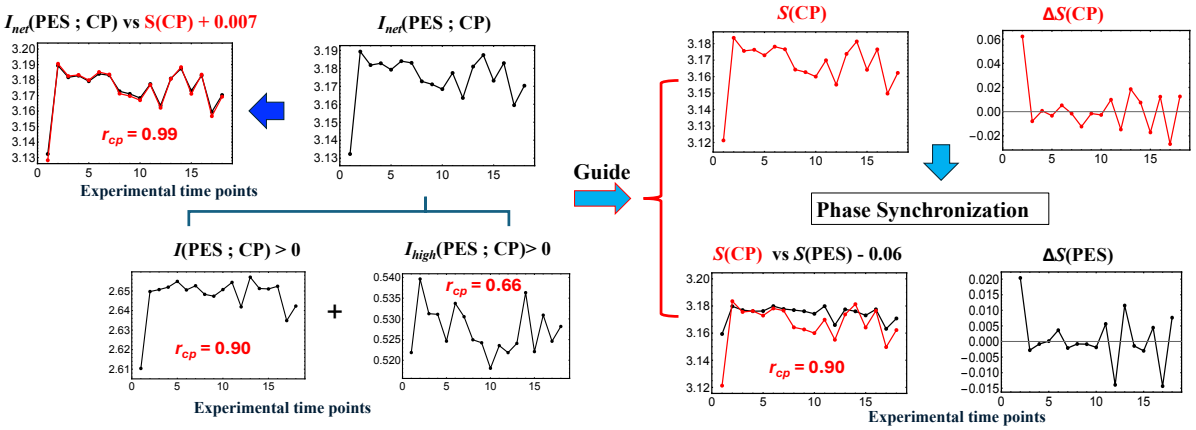

B) Phase synchronization: HRG-stimulation

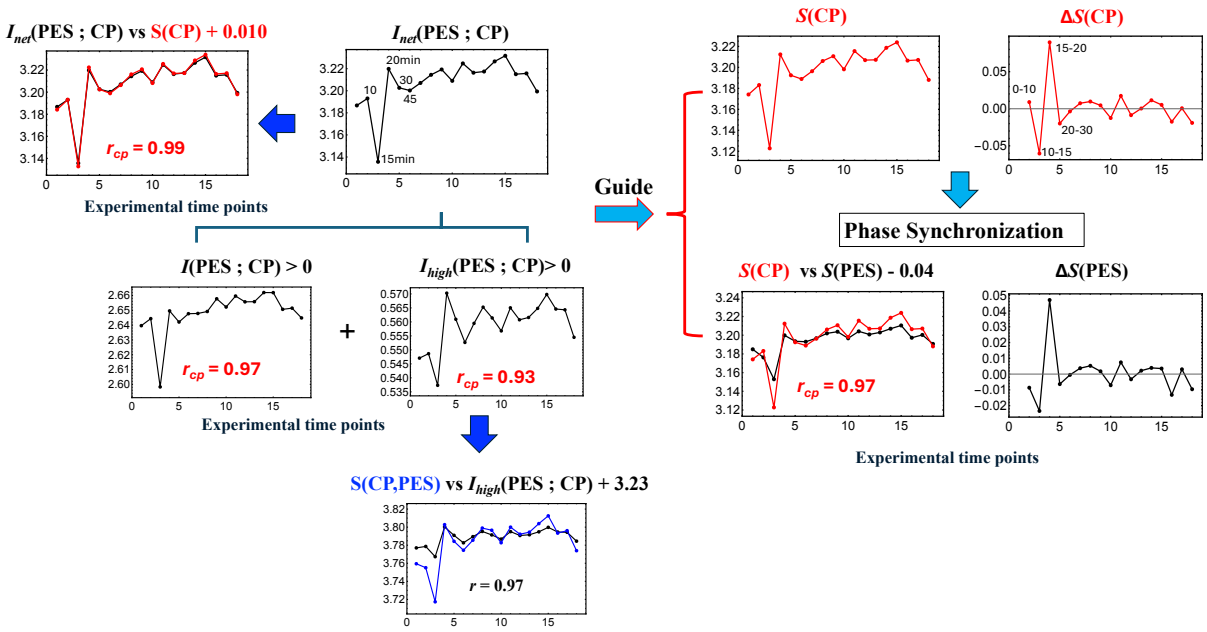

Figure 6: Thermodynamic Phase Synchronization of CP with the Rest of WES (PES). A) EGF stimulation. B) HRG stimulation. The net mutual information exhibits a near-perfect temporal correlation with the dynamics of S(CP) (r_{cp} = 0.99), indicating that the CP guides synchronization with the PES, supporting fundamental phase synchronization between CP and PES. Additionally, the positive higher-order information reveals nonlinear interdependencies within the WES, capturing both redundant and synergistic interactions (see **section 2.3**).

2.5 CP Acts as Maxwell's Demon in Early HRG-Signaling Response

Unlike EGF, which induces early disorder (0–10 min), HRG triggers a distinct critical transition, synchronizing ordered and disordered phases across all information-thermodynamic metrics from 10 to 20 minutes. As shown in **Figures 5B** and **6B**, the CP acts as a Maxwell demon [Parrondo et al., 2015], regulating information flow and maintaining adaptable chromatin states (see **section 2.6** for details).

The CP, functioning as a Maxwell's demon, orchestrates gene expression and cell fate through three distinct phases:

Phase 1: Preparation (10–15 minutes): The CP synchronizes with the PES to minimize the entropies of both CP and PES genes, establishing their initial states. Biologically, this synchronization sustains the upregulation of AP-1 complex genes and coordinates the activation of their downstream targets, ensuring proper assembly and functionality of AP-1 components (see **section 2.4**).

Phase 2: Measurement (15–20 minutes): Synchronization between the CP and PES initiates the measurement process, leading to the largest increases across all information-thermodynamic metrics, including CP and PES entropy, as well as standard, higher-order, and net mutual information.

Phase 3: Feedback and Critical Transition (20–30 minutes) - Utilizing the net information obtained in Phase 2, the CP reorganizes and provides feedback to the PES, triggering a critical transition at 20 minutes in the WES. This feedback-driven reorganization reduces system entropy, driving the system into a new ordered state.

Further details are provided below:

Phase 2: Measurement Phase (15–20 Minutes)

1. Highest Increases in CP Entropy, PES Entropy, and Net Mutual Information

As shown by the 15- and 20-minute data points in Figure 5B (or Figure 6B), CP genes acquire the most information about PES during the measurement phase. Processing and storing this information raises CP entropy due to thermodynamic costs. This phase sees the largest increases in both standard and higher-order MI, driving net MI from its 15-minute minimum. Notably, the surge in higher-order MI underscores strong nonlinear interdependencies between CP and PES.

Figure 6B shows that higher-order MI strongly correlates with the joint entropy S(CP,PES) ($r = 0.97$). As total uncertainty increases, more states become accessible, broadening the system's global search space and amplifying structured interactions between CP and PES. The positive higher-order MI reflects both synergy (emergent collective information) and redundancy (overlapping information) (see **section 2.3**), enabling the CP to encode information about PES despite rising global uncertainty. This open thermodynamic phase synchronization, led by CP genes, is a hallmark of complex systems, where localized organization persists in high-entropy environments, supporting robust information processing.

Note: Typically, in measurement scenarios [Parrondo et al., 2015], the entropy of the measured system S(PES) decreases as it loses information to the CP, increasing internal order. However, in this phase, S(PES) instead rises due to phase synchronization between the CP and PES, during which the PES absorbs energy from the environment. This absorbed energy, whether heat, free energy, or chemical substrates, offsets the entropy reduction caused by information loss to the CP. Consequently, phase synchronization is sustained through exchanges with the cell's external environment (see **section 2.4**).

The synchronized metrics in Phase 2 lay the foundation for the feedback process in Phase 3, driving the system's critical transition to a new cell state.

Phase 3: Feedback and critical transition

1. Initiation of Critical Transition (20–30 Minutes):

During this interval, the CP's decreasing entropy induces a corresponding drop in PES entropy through phase synchronization, facilitated by exchange entropy and information flow with the environment. Concurrently, declines in both standard MI and higher-order MI reduce net MI, suggesting that the CP is leveraging information from Phase 2 to guide the PES through a critical transition. Notably, the timing of this CP feedback at 20 minutes aligns with a genome-wide transition, as shown by expression flux analyses [Tsuchiya et al., 2023a] and PCA [Zimatore et al., 2021].

2. Stabilization into New States After 30 minutes:

After 30 minutes, fluctuations in S(CP) and S(PES), and net mutual information suggest that both CP and PES are settling into stable, reorganized states. Notably, between 30 and 45 minutes, the bimodal CP dissipates, and by 60–90 minutes, a new CP emerges, indicating the establishment of a new state (see **section 2.6**).

2.6 Maxwell's Demon Functioning as Rewritable Chromatin Memory

J. Krigerts et al. (2021) recently investigated experimentally critical transitions in chromatin dynamics during early differentiation in HRG-stimulated MCF-7 breast cancer cells, focusing on pericentromere-associated domains (PADs). They identified two key critical transitions:

1. **First Critical Transition (15-20 Minutes)**: Following HRG treatment, PADs undergo a "burst," dispersing from their clustered state near the nucleolus. This dispersal coincides with the activation of early response genes, such as c-fos, fosL1, and c-myc, which initiate the differentiation process. During this phase, repressive chromatin structures unravel, and active chromatin regions become more accessible, marking a significant step in genome reorganization..
2. **Second Critical Transition (Around 60 Minutes):** The second transition involves further chromatin alterations, including increased transcription of long non-coding RNAs (lncRNAs) from PADs. This supports additional chromatin unfolding and

genome rewiring, which are essential for establishing and maintaining differentiation, ultimately determining a stable and functional cell fate.

In this section, we explore the thermodynamic mechanisms underlying these two critical transitions in chromatin dynamics. To achieve this, we analyze the metric parameter *nrmsf* (equation (1)), which indicates the self-organization of the whole expression system (WES) into distinct response domains (critical states) separated by a critical point (CP) (**Figure 1**). This parameter quantifies the temporal variability of gene expression as a time-independent measure.

Zimatore et al. [Zimatore et al., 2021] showed that *nrmsf* effectively captures time-based variability in gene expression, and that principal component (PC) scores from temporal whole-expression data accurately predict each gene's *nrmsf*. The second and third components (PC2 and PC3) reflect chromatin's structural flexibility, closely linked to folding and unfolding during the cell-fate, guiding critical transition in HRG-stimulated MCF-7 cells. Notably, a one-order-of-magnitude increase in the variance explained by PC2 - the main direction of displacement from the genome attractor (GA) - coincides with peri-centromeric body splitting and chromatin unfolding, exposing new genomic regions to polymerases [Krigerts et al., 2021]. Since PC2 mirrors *nrmsf* changes in oscillating-mode genes (OMGs) [Tsuchiya et al., 2023a], these findings connect chromatin dynamics to thermodynamic properties such as Shannon entropy.

To formulate the Shannon entropy associated with chromatin dynamics, we transform the original gene expression probability distribution into an *nrmsf* probability distribution (see **Appendix** for mathematical description). **Figure 7** illustrates this workflow: starting with the raw expression data, we systematically bin gene expression values into m discrete *nrmsf* categories. These categories serve as 'logical states,' while the actual gene expression values populating each bin represent the 'physical states' embedded within those logical categories.

This approach aligns with the concept of entropy decomposition into logical and physical states, as discussed by Maroney [Maroney, 2009] in the context of generalizing Landauer's principle. By establishing *nrmsf* bins as logical states, we create a structured, higher-level framework that organizes the more granular expression levels (physical states). In other words, the logical states (i.e., *nrms*f bins) capture the distribution of uncertainty at a coarser scale, while the

physical states (the actual gene expression values within each bin) account for the residual uncertainty at finer resolution.

To ensure the robustness of our entropy estimates, we employ a convergence-based approach described in **Figure 4**. This method stabilizes the assessment of uncertainty by redistributing the fundamental entropy element, $-p(x_i(t_j))ln(p(x_i(t_j)))$, across the *nrmsf* bins. Each individual expression value ($x_i(t_j)$) contributes to the entropy at the logical (bin) level, allowing us to map local gene expression dynamics onto the *nrmsf* probability distribution.

Through this transformation, we gain insights into how chromatin state changes influence the distribution of gene expression. By viewing entropy both at the logical (*nrmsf* bin) and physical (individual expression values) scales, we move beyond raw probability distributions to an information-theoretic description that captures dynamic variability and regulatory mechanisms at play in chromatin dynamics.

Note that we use the workflow in **Figure 7** to analyze chromatin dynamics. From a convergence perspective, transforming the entropy element using a one-dimensional frequency table is simpler than the two-dimensional approach described in the **Appendix**, which accounts for both logical and physical states simultaneously.

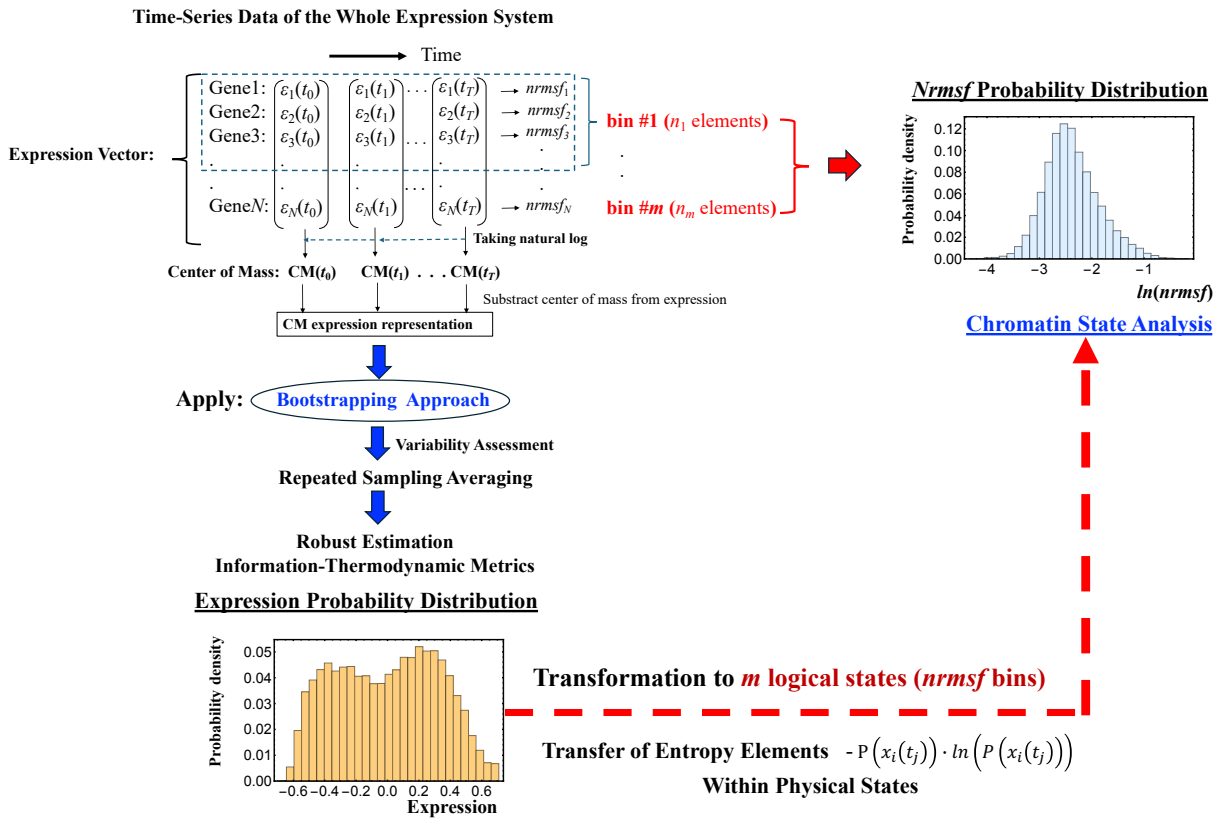

Figure 7: Information-Theoretic Workflow for Transforming Gene Expression into nrmsf Probability Distributions. This figure illustrates the workflow for transforming gene expression probability distributions into *nrmsf* probability distributions, reflecting entropy changes associated with chromatin states. The process begins with temporal gene expression data of the whole expression system (WES), which includes the CP as the regulatory hub and the peripheral expression system (PES) (refer to **Figure 1**). Mutual information metrics, I_{net}(CP;PES) = I(CP;PES) + I_{high}(CP;PES), are calculated to quantify the interaction and coherence between these subsystems, providing an information-theoretic perspective on gene regulation (see **section 2.3**). A bootstrapping approach (**Figure 4**) is applied to assess the variability and uncertainty of these metrics, ensuring robustness in the analysis. Finally, entropy elements, represented as $-p(x_i(t_j))ln(p(x_i(t_j)))$, are transformed into an *nrmsf*-based probability distribution. The *nrmsf* bins represent logical states, while the original gene expression values within each bin correspond to the underlying physical states. By incorporating this logical/physical state perspective, the transformation reveals dynamic variability and chromatin state changes. For additional details, refer to **Figure 8**.

Figure 8 depicts the temporal variations in Shannon entropy linked to chromatin dynamics across the WES for EGF- and HRG-stimulated MCF-7 cells:

1. **EGF-stimulated MCF-7 cells (Figure 8A)**: This panel shows the temporal changes in Shannon entropy linked to chromatin dynamics in EGF-stimulated MCF-7 cells. Within the specified range (-2.64 < *ln*(*nrmsf*) < -2.52; **Fugure 1**), a CP-like (critical point-like) bimodal pattern in entropy changes occasionally appears, suggesting transient critical behaviors in chromatin organization. During these intervals, positive entropy changes ($\Delta S > 0$) are associated with chromatin unfolding, while negative entropy changes ($\Delta S < 0$) are associated with chromatin folding.

   Although these CP-like bimodal patterns emerge intermittently, such as during the 0–10 and 20–30 minute windows, they dissolve and reappear without inducing a sustained critical transition or altering cell fate. This implies that the conditions needed to activate a Maxwell's demon-like mechanism are not fully met. Notably, these chromatin fluctuations are driven by CP–PES phase synchronization, underscoring the role of thermodynamic interactions in maintaining dynamic chromatin states despite the absence of a full critical transition.
2. **HRG-stimulated MCF-7 cells (Figure 8B)**: The scenario of Maxwell's demon-like chromatin memory progresses through distinct phases. During the initial 0-10 minutes, a CP-like bimodal pattern (-2.55 < *ln*(*nrmsf*) < -2.44; **Figure 1**) emerges. At 10-30 minutes, a global fold-unfold coherent transition occurs around *ln*(*nrmsf*) = -3.11 to -3.04, involving Maxwell's demon-like behavior (see **section 2.5**). This phase acts as a rewritable chromatin memory, reflecting changes in double-well potential profiles (**Figure 9**). At 30-45 minutes, the CP pattern dissolves, likely preparing the system for a new stable genomic state of the WES. At 60–90 minutes, CP formation reappears, suggesting a cell-fate change consistent with the second transition described by Krigerts et al. (2021). Beyond 90 minutes, CP-like bimodal patterns continue to form and dissolve intermittently, indicating sustained chromatin adaptation under HRG stimulation.

Using the *nrmsf* metric, Shannon entropy reveals chromatin folding and unfolding dynamics. EGF stimulation repeatedly dissolves and reinitiates reversed CP bimodal pattern formations without inducing cell fate changes, while HRG stimulation facilitates stable CP formation and cell fate transitions driven by Maxwell's demon-like chromatin memory at 10-30 min. The CP's role, measuring genomic states, orchestrating entropic and informational dynamics, and reorganizing chromatin, demonstrates its active function in encoding, decoding, and re-encoding chromatin configurations. This process aligns with the concept of memory storage

and rewriting within a dynamically regulated, thermodynamically controlled genomic landscape (**Figure 9**).

A) EGF-Stimulation

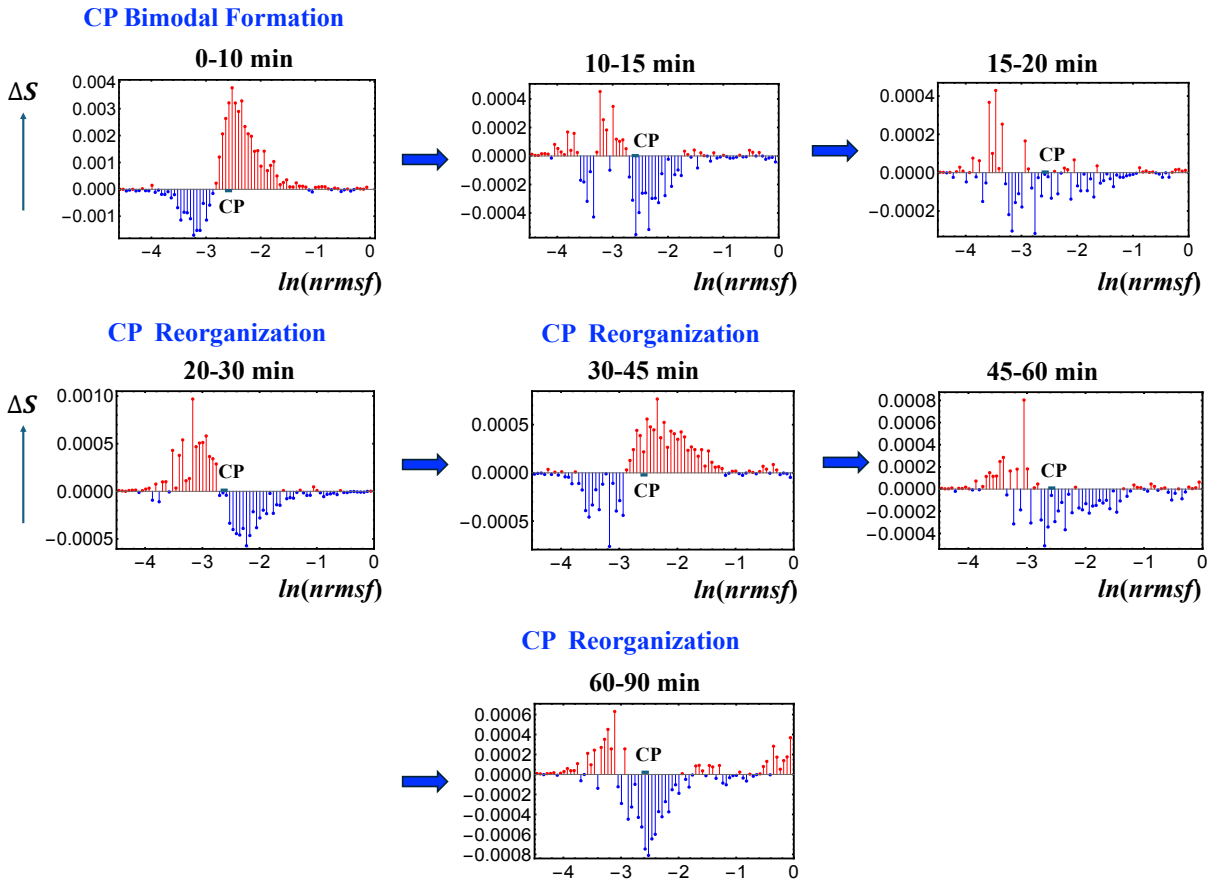

B) HRG-Stimulation

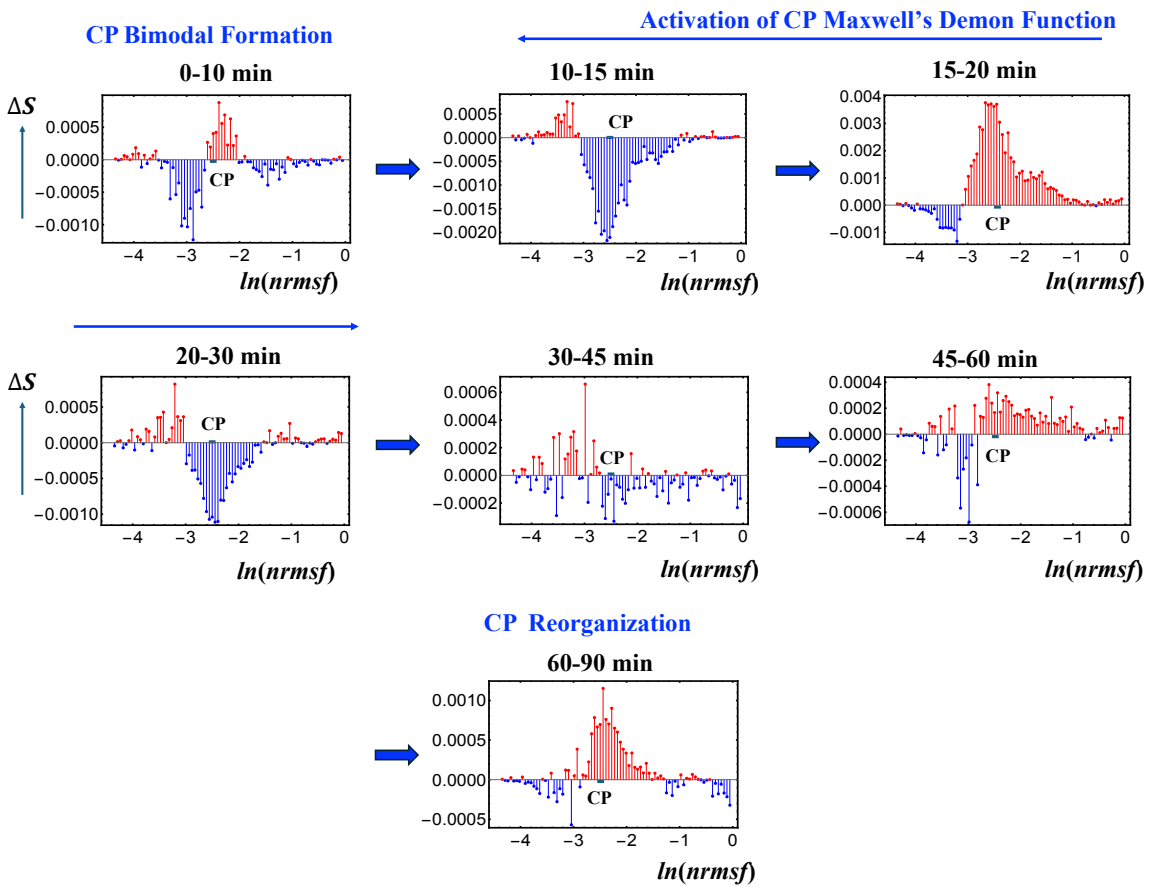

Figure 8: Chromatin Dynamics and CP Formation Across Temporal Entropy Changes

Temporal changes in Shannon entropy associated with chromatin dynamics are plotted against the natural logarithm of *nrmsf* (80 bins) in EGF- **(A)** and HRG-stimulated **(B)** MCF-7 cells. The Critical Point (CP), indicated by the bold black solid line, marks regions where singular bimodal behavior occurs within the range -2.64 < *ln*(*nrmsf*) < -2.52 for EGF stimulation and -2.55 < *ln(nrmsf*) < -2.44 for HRG stimulation (see **Figure 1**). Under EGF stimulation, intermittent CP bimodal patterns emerge at specific intervals (e.g., 0–10 and 20–30 minutes) but repeatedly dissolve without triggering a critical transition, resulting in no cell fate change.

In contrast, HRG stimulation initially produces a CP bimodal pattern during the 0–10 min period, which transitions into a global coherent fold–unfold chromatin change between 10–30 minutes. This is followed by the re-formation of CP states between 60–90 minutes, aligning with a cell fate transition. These results highlight cyclical chromatin organization states driven by CP–PES phase synchronization and thermodynamic interactions, including Maxwell's demon-like chromatin memory effects.

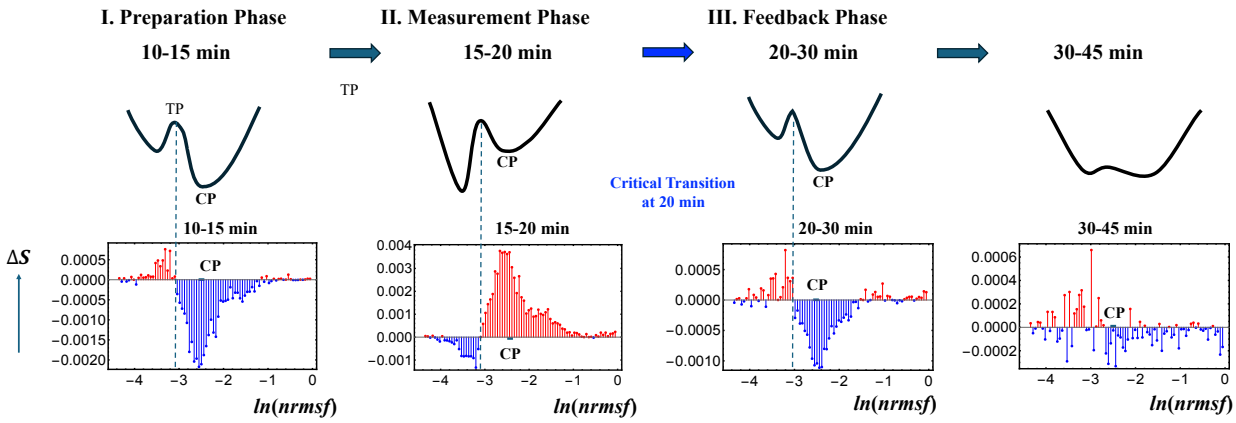

Figure 9: Schematic Representation of a Maxwell's Demon Double-Well Potential Profile. This figure illustrates a conceptual double-well potential landscape representing chromatin dynamics, highlighting the Maxwell's demon-like behavior of the CP within the range -2.55 < *ln*(*nrmsf*) < -2.44. Each well corresponds to a distinct chromatin state, such as folded or unfolded chromatin, separated by a potential barrier. The transition point (TP) occurs around ln(nrmsf) = -3.15 to -3.00, where chromatin restructuring takes place. Chromatin remodeling dynamics are visually represented by up (red) and down (blue) arrows, reflecting the oscillatory behavior of chromatin folding and unfolding, dynamically centered around the CP. After 30 minutes, the potential barrier almost disappears, suggesting inactive Maxwell's demon function with a loss of coherent chromatin state. The vertical axis represents changes in Shannon entropy associated with chromatin remodeling, while the horizontal axis represents the value of *ln(nrmsf)* (refer to the main text for details).

3. Discussion: Biophysical Implications

Our findings highlight the genome as an open thermodynamic system operating far from equilibrium. Gene expression and chromatin organization are not static; they are maintained through continuous energy dissipation, allowing cells to adapt flexibly to changing environments. This perspective reveals how biological systems achieve coherence and stability despite external perturbations and how the interplay between chromatin structure and gene regulation can be explained under the framework of a dissipative thermodynamics.

From a biomedical standpoint, this thermodynamic perspective has substantial implications. By elucidating the principles governing how cells adopt and maintain distinct fates, we gain insights into processes such as cancer progression, metastasis, and therapeutic resistance. Manipulating the genome's regulatory architecture—particularly the "CP," a critical gene set that functions as a central regulatory hub—may offer strategies for reprogramming cell states.

For instance, restricting undesirable plasticity in cancer cells or guiding stem cells toward more favorable differentiation pathways could offer new strategies for improved therapeutic interventions.

In Discussion section, we further expand our findings and discuss the potential for controlling the dynamics on the the fate of cancer cells in three key aspects: 1) order parameter of phase synchronization, 2) autonomous genome computing and 3) genome intelligence (GI).

1) Existence of Order Parameter of Phase Synchronization

We explore the emergence of an order parameter for phase synchronization, integrating expression flux analysis [Tsuchiya et al., 2020, 2022, 2023a] with genomic-thermodynamic phase synchronization. Under HRG stimulation, during the critical transition, the CP undergoes a substantial change in all information-thermodynamic metrics, including entropy, both at the CP and in the PES (whole expression system without the CP genes) (**Figure 5B**). Additionally, there is a marked increase in self-flux (effective force) at both the CP and the genome attractor (GA) (**Figure 10A**). This critical transition induces a drastic system-wide shift, where all statistical measures/parameters describing the state become highly correlated, effectively collapsing the dynamical space into a binary regime: CP activation (HRG) vs. no CP activation (EGF). Consequently, every computed index converges under a unified critical framework, suggesting that the dynamics of phase transitions not only drive biological coherence (pulse phase in biphasic induction of AP-1 complex [Nakakuki at al. 2010]) but also integrate diverse analytical metrics into a single, self-operating system.

Figure 10 provides evidence of this collapse in dynamical space, showing the concurrent occurrence of three types of phase synchronization at the CP: entropy-based thermodynamics (ΔS(CP)), CP force-like dynamics (self-flux), and GA self-flux. This finding indicates that thermodynamic (entropy) and mechanical-like forces jointly drive the establishment and propagation of global phase coherence [Ott and Antonsen, 2008]. Their synergy implies that neither force alone can fully account for large-scale synchronization; rather, their combined action underpins robust, system-wide coherence, highlighting the integrative nature of genomic regulation in cancer cells.

A key aspect of the emergent is the development of a robust order parameter that quantitatively characterizes phase synchronization. Analogous to the Kuramoto order parameter [Kuramoto,

1975; Strogatz, 2000], this scalar measure ranges from near-zero (indicating incoherent or random phase relationships) to one (denoting near-perfect synchrony). The order parameter thus encapsulates the degree of phase alignment among the CP and GA, serving as a macroscopic indicator of the (critical) phase transition. As the CP and GA becomes increasingly synchronized, the order parameter rises sharply, marking the transition from a disordered to an ordered state - a signature hallmark of self-organized critical (SOC) control in whole expression.

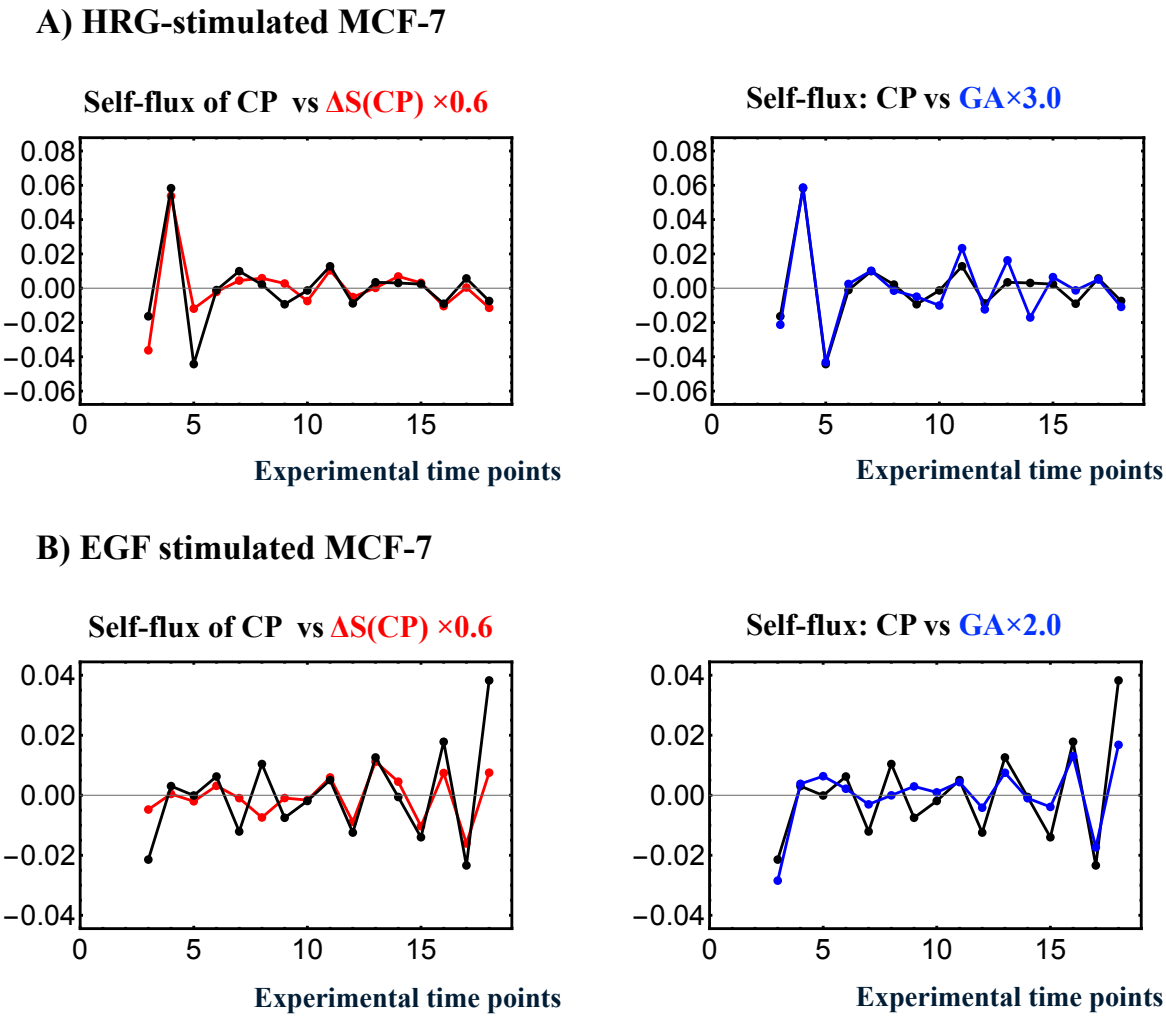

Figure 10. Concurrent occurrence of entropy-based thermodynamic synchronization and force-like dynamical synchronization. In HRG stimulation (A) and EGF stimulation (B), the left panel shows the phase synchrony between self-flux (a dynamical system measure) and entropy change ΔS(CP) (a thermodynamic measure) for CP genes, while the right panel presents the self-flux of the CP and genome attractor (GA). Here, the self-flux of the CP and GA is defined as the second difference from its overall temporal average value: $\varepsilon(t_{j+1}) - 2\cdot\varepsilon(t_j) + \varepsilon(t_{j-1})$, where $\varepsilon(t_j)$ represent expreesion of the

center of mass of CP genes or GA at $t = t_j$. The change in CP entropy is given by its first difference: $S(CP(t_j)) - S(CP(t_{j-1}))$.

Phase synchrony becomes apparent after the 10-minute interval, with ΔS(CP) after 10–15 minutes and self-flux after 0–10–15 minutes. HRG stimulation, which induces a critical transition, shows stronger phase synchrony compared to EGF stimulation, where no critical transition occurs. In contrast, in the EGF case, the early-time CP formation-deformation cycle suggests that it leads to a weak phase synchrony among CP self-flux, its entropy change, and GA self-flux (see **Figure 8A**).

2) Autonomous Genome Computing as a Conceptual Framework

Recent advances suggest that genomic DNA is not merely a static blueprint but a dynamic, computationally capable system—a concept we refer to as "genome computing." Here, "computation" describes the genome's autonomous potentiality to integrate diverse regulatory inputs, store adaptive information, and transition between functional states in a context-dependent manner. This perspective offers a unifying framework to understand the nonlinear, adaptive behaviors that regulate gene expression, drive cell differentiation, and govern cellular responses to external cues.

One key insight is that time-dependent transitions in genomic states can be modeled using kinetic equations with cubic nonlinearity, derived from symmetry arguments in thermodynamics. This nonlinearity arises from changes in translational and conformational entropy within large DNA molecules interacting with their associated ionic environments. Experimentally observed chromatin reorganizations support this perspective, suggesting that genomic architecture is continuously tuned to explore and settle into favorable configurations.

The symmetry with cubic nonlinearity mirrors excitability phenomena observed in neuronal systems, as described by the FitzHugh-Nagumo [FitzHugh, 1955; Nagumo et al., 1962] and Hodgkin-Huxley [Hodgkin and Huxley, 1952] frameworks. While these parallels remain conceptual, they underscore a shared principle: nonlinear systems, whether neural or genomic, can exhibit threshold-dependent switching between stable states.

Recent evidence clearly demonstrates that genome-sized DNA exhibits a bimodal free energy profile [Yoshikawa et al., 2000; Iwaki et al., 2003; Nakai et al., 2005; Mayama et al., 2007;

Estévez-Torres et al., 2011; Yoshikawa et al., 2011; Nishio et al., 2020]. This bimodal symmetry inherently implies cubic nonlinearity in the reaction kinetics, which arises from the functional derivative of the free energy [Yoshikawa, 2002；Takenaka et al., 2008: Nagahara and Yoshikawa, 2010; Kanemura et al., 2018].

At the heart of these transitions lies the occurrence of the Critical Point (CP). While its precise composition remains to be fully delineated, existing evidence suppots that specific genomic regions consistently orchestrate large-scale regulatory shifts. As cells approach critical decision points—such as lineage commitment—the CP emerges from bimodal states, toggling chromatin configurations between more and less active forms. Observations of pericentromere-associated domain (PAD) rearrangements and chromatin remodeling [Krigerts et al., 2021] further support the notion that the CP governs these critical transitions, effectively "choosing" among distinct genomic states.

These transitions can be conceptualized through an energy landscape perspective, where changes in translational and conformational entropy reshape the free energy landscape, favoring certain pathways over others. Analogies with Ginzburg-Landau theory [Ginzburg and Landau, 1965] highlight the importance of identifying order parameters (e.g., chromatin compaction or gene network states) and recognizing that critical transitions occur when specific thresholds are crossed. Our self-organized criticality (SOC) provides another useful framework: the genome, via the CP, naturally tunes itself to critical points, maintaining a balance between order and flexibility. Acting as rewritable chromatin memory, the CP plays a role akin to Maxwell's demon, selectively promoting transitions that reduce uncertainty and drive the system toward coherent and functionally relevant states.

This notion of "genome computing" does not imply that the genome functions like a digital processor with discrete inputs and outputs. Instead, genome computing is characterized by autonomous, decentralized super-information processing. It reflects a continuous, adaptive reshaping of genomic states, where "memory" is encoded in the genome's ability to revisit specific conformations, and "logic" emerges from network interactions that drive transitions toward or away from stable regulatory configurations.

In conjunction with the genomic-thermodynamic mechanism, understanding how the CP functions as a central process hub to orchestrate the complex spatiotemporal self-organization of the genome will elucidate fundamental principles governing cell fate, development, and

stress responses. This knowledge should ultimately inspire innovative approaches in regenerative medicine, cancer therapy, and synthetic biology.

3) Genome Intelligence (GI) Supported by Autonomous Genome Computing

On a more theoretical level, the concept of GI builds upon the computational principles of genome computing to describe the genome's ability to exhibit integrated, adaptive, and memory-like behavior. Here, intelligence refers to a minimal form of integrated responsiveness, where the genome does not merely react to environmental stimuli but incorporates these stimuli into its regulatory framework, enabling adaptation and future decision-making.

Integrated Information Theory (IIT), initially developed to explain consciousness in neural systems, provides a useful framework for understanding intelligence in biological systems. The fundamental challenge of IIT lies in the integration of external informative stimuli into the structure of the 'intelligent agent,' leading to the emergence of a 'memory' of the stimulus. This stands in contrast to non-intelligent sensors (e.g., a photodiode), whose structure remains unchanged by their interaction with the sensed stimulus.

As demonstrated by Niizato et al. (2024), IIT extends beyond neural systems to describe integrated information within molecular and cellular systems, where complex interactions produce irreducible wholes. Applying this principle to the genome, GI arises from the integration of external signals into chromatin configurations, regulatory networks, and gene expression states. This capacity for integration, persistence, and reconfiguration distinguishes the genome as an autonomous intelligent system.

While genome computing describes the mechanisms by which the genome processes and integrates information, GI emphasizes the emergent properties of this system. Intelligence reflects the genome's ability to actively discriminate between different environmental or internal states, enabling a nuanced understanding of the cellular context. By integrating these states into its chromatin structure and regulatory networks, the genome establishes a foundation for dynamic memory, encoding past experiences to inform future actions. Furthermore, this intelligence allows the genome to adaptively guide transitions to future regulatory configurations, ensuring cellular responses remain both coherent and flexible in the face of changing conditions.

This mechanism corresponds to the emergence of a set of strongly correlated subsets of genes, as described by Dynamic Network Biomarker (DNB) theory [Aihara et al., 2022]. DNB theory highlights how such subsets act as early indicators of critical transitions, emphasizing the coordination of gene dynamics during these pivotal moments. Additionally, this behavior is tied to an increase in the power of a minor principal component orthogonal to the "tissue attractor" main principal component, as shown by Zimatore et al. [Zimatore et al., 2021]. These findings underline the genomic system's ability to consolidate information across scales, creating a dynamic regulatory network that integrates both structural and functional changes.

For example, in supercritical states, the genome demonstrates a heightened sensitivity to perturbations, enabling rapid transitions that propagate across the chromatin landscape. These transitions are not random but are orchestrated by the OMG (oscillatory mode genes)–CP–GA (critical point–genome attractor) network [Tsuchiya et al., 2023a], which align the genome's response with the needs of the cell. Such behavior mirrors the minimal criteria for intelligence outlined in IIT, where integrated information is both created and used to maintain system coherence.

In principle, genome-based systems could be engineered to construct dynamic logical networks, such as non-binary finite state machines [Yeo et al., 2007; Moon et al., 2012; Doe and Smith, 2023]. These systems replicate genome intelligence in synthetic or computational contexts by mimicking critical-state hubs, such as the OMG–CP–GA network. These hubs reflect the genome's inherent capacity for adaptation and self-organization. As noted by Zimatore et al. [Zimatore et al., 2021], subsets of genes driving these transitions are enriched in chromatin-folding dynamics, reinforcing the idea that genomic intelligence emerges from its ability to orchestrate large-scale structural and regulatory changes.

Ultimately, GI reframes our understanding of the genome as a dynamic, adaptive, and integrative system. By uniting computational and thermodynamic principles with biological mechanisms, this concept provides a foundation for exploring how genomes encode past experiences, adapt to changing conditions, and guide cellular behavior. This perspective has profound implications for fields ranging from regenerative medicine to synthetic biology, where leveraging the intelligent properties of the genome could revolutionize how we design and manipulate living systems.

4. Conclusion

Our study demonstrates that genomic regulation can be understood through the lens of open stochastic thermodynamics. Rather than existing at thermodynamic equilibrium, gene expression operates far from equilibrium, with continuous energy dissipation enabling dynamic regulation, adaptability, and responsiveness to external cues. By examining the roles of critical point (CP) genes and the whole expression system (WES) in MCF-7 breast cancer cells, we present a thermodynamic framework that explains how biological systems autonomously maintain coherence, stability, and flexibility in their gene expression profiles.

Key insights from our findings include the thermodynamic phase synchronization of CP genes with the genome, the distinct roles of the CP under different stimuli, and the presence of positive high-order mutual information. The latter highlights nonlinear interdependencies, enhancing both synergy (emergent collective information) and redundancy (overlapping information) beyond the framework of the pairwise framework of interactions among genes.

For example, under epidermal growth factor (EGF) stimulation, the CP remains passive, preserving stability without transitioning into a new state. In contrast, under heregulin (HRG) stimulation, the CP “reads” and redistributes information to guide a global transition in gene expression. In other words, the genome “learns” from environmental signals, processes that information, and then reprograms its overall state—a phenomenon that can be described as “Genome Intelligence (GI)”.

On a broader level, these computational dynamics support the concept of GI, where the genome exhibits emergent properties such as the ability to discriminate between environmental states, integrate signals into its structural framework, and adaptively guide future regulatory transitions. This emergent intelligence reflects the genome’s capacity to store "memory" of past states and utilize this information to navigate complex decision-making landscapes. These insights bridge classical molecular genetics with nonequilibrium thermodynamic and computational principles, providing a holistic view of genome regulation.

Our findings open new avenues for understanding disease progression, guiding regenerative medicine, and informing innovative cancer therapies. For example, the CP’s ability to dynamically “compute” and integrate signals highlights opportunities for targeting critical regulatory hubs in cancer treatment or leveraging genomic intelligence in synthetic biology to design adaptive, programmable cellular systems.

From a global perspective, this integration of genome computing and intelligence inspires the development of machine learning tools modeled on cell fate transition dynamics. Physics-

Informed Neural Networks (PINNs), as described by Cai et al. (2021), offer a promising framework for incorporating physical principles into neural network architectures to replicate the behavior of biological systems. Similarly, Hopfield networks, as noted by Krotov [Krotov, 2023], demonstrate how network correlations can encode emergent behavior, much like genomic systems encode adaptive regulatory transitions. By applying these computational principles as hyper-parallel autonomous decentralized systems, we can enhance both biological understanding and machine learning, paving the way for models that seamlessly integrate thermodynamic, computational, and biological insights.

5. Material

Microarray data for the activation of ErbB receptor ligands in human breast cancer MCF-7 cells by EGF and HRG; Gene Expression Omnibus (GEO) ID: GSE13009 (N = 22277 mRNAs; for experimental details see [Saeki et al., 2009]) at 18 time points: $t_1 = 0$, $t_2 = 10$, 15, 20, 30, 45, 60, 90 min, 2, 3, 4, 6, 8, 12, 24, 36, 48, $t_T = 18 = 72$h. The robust multichip average (RMA) was used to normalize expression data for further background adjustment and to reduce false positives [Bolstad et al., 2003; Irizarry et al., 2003; McClintick and Edenberg, 2006].

6. Apenndix: Mathematical description of Chromatin Entropy

As illustrated in **Figure 7**, we transformed the expression distribution into the normalized root mean square fluctuation (*nrmsf*) probability distribution—an entropy decomposition approach analogous to the logical/physical state framework described by Maroney [Maroney, 2009]. To provide a mathematical perspective, we describe chromatin entropy by showing how the Shannon entropy of the Whole Expression System (WES), defined in equation (2), into "logical states" corresponding to *nrmsf* bins as follows:

$$S\left(X(t_j)\right) = -\sum_i P\left(x_i(t_j)\right) ln\left(P\left(x_i(t_j)\right)\right)$$

$$= -\sum_m \sum_{x_i \in m} P(x_i(t_j)|m) \cdot P(m) \cdot ln\left(P(x_i(t_j)|m) \cdot P(m)\right)$$

$$= -\sum_m \sum_{x_i \in m} P(x_i(t_j)|m) \cdot P(m) \cdot \left(ln\left(P(x_i(t_j)|m)\right) + ln(P(m))\right)$$

$$= \quad S(M) + \sum_m P(m) \cdot S\left(Y_m(t_j)\right). \tag{16}$$

Here, the probability $P(x_i(t_j))$ of gene x_i being expressed at time t_j can be factored into 1) the probability of selecting a logical state m, $P(m)$, and 2) the probability of the physical state $x_i(t_j)$ within that logical state, $P(x_i(t_j)|\mathrm{m})$, such that $P(x_i(t_j)) = P(x_i(t_j)|\mathrm{m}) \cdot P(m)$. The sum of probabilities within each logical state satisfies $\sum_{x_i} P\left(x_i(t_j)\middle|m\right) = 1$ at time t_j.

The entropy of the whole expression system, S(WES), is thus expanded in terms of $S(M)$, the entropy associated with the distribution of logical states, and $S(Y_m(t_j))$, which represents the entropy of the physical states (gene expression levels) within the mth logical state:

$$S(M) = -\sum_m P(m) \cdot ln\left(P(m)\right), \tag{17}$$

and

$$S\left(Y_m(t_j)\right) = -\sum_{x_i \in m} P(x_i(t_j)|m) \cdot ln\left(P(x_i(t_j)|m)\right). \tag{18}$$

Author Contribution

MT: Conceptualization (Lead); Formal Analysis and Software; Methodology; Writing – Original Draft; Writing – Review & Editing

KY: Conceptualization (Supporting); Writing – Review & Editing

AG: Conceptualization (Supporting); Writing – Review & Editing

Acknowledgments

MT thanks Prof. Paul Brazhnik for his insightful discussions and the SEIKO Life Science Laboratory, Osaka, Japan, for its invaluable support during this research. He is also grateful to his family—Ms. Takako Tsuchiya, Drs. Kimiko & Kazumi Tsuchiya, and Dr. Harry Taylor—for their constant encouragement. Special thanks go to Dr. Dasaku Ikeda for his lifelong inspiration and to Ms. Satoko Takeda & Ms. Hisami Spector jfor their kind and heartfelt support.

References

Adami, C. (2004). Information theory in molecular biology. Phys. Life Rev., 1, 3–22. https://doi.org/10.1016/j.plrev.2004.01.002

Aihara, K., Liu, R., Koizumi, K., Liu, X., & Chen, L. (2022). Dynamical network biomarkers: Theory and applications. Gene, 808, 145997. https://doi.org/10.1016/j.gene.2021.145997

Annby-Andersson, B., Bhattacharyya, D., Bakhshinezhad, P., Holst, D., De Sousa, G., Jarzynski, C., Samuelsson, P., & Potts, P. P. (2024). Maxwell's demon across the quantum-to-classical transition. Phys. Rev. Res., 6, 043216. https://doi.org/10.1103/PhysRevResearch.6.043216

Bak, P., Tang, C., & Wiesenfeld, K. (1987). Self-organized criticality: An explanation of the 1/f noise. Phys. Rev. Lett., 59, 381–384. https://doi.org/10.1103/PhysRevLett.59.381

Bak, P., Tang, C., & Wiesenfeld, K. (1988). Self-organized criticality. Phys. Rev. A, 38, 364–374. https://doi.org/10.1103/PhysRevA.38.364

Bak, P., & Chen, K. (1991). Self-organized criticality. Sci. Am., 264, 46–53.

Barato, A. C., & Seifert, U. (2014). Unifying three perspectives on information processing in stochastic thermodynamics. Phys. Rev. Lett., 112, 090601. https://doi.org/10.1103/PhysRevLett.112.090601

Bennett, C. H. (2003). Notes on Landauer's principle, reversible computation, and Maxwell's demon. Stud. Hist. Philos. Mod. Phys., 34, 501–510. https://doi.org/10.1016/S1355-2198(03)00039-X

Bérut, A., Arakelyan, A., Petrosyan, A., Ciliberto, S., Dillenschneider, R., & Lutz, E. (2012). Experimental verification of Landauer’s principle linking information and thermodynamics. Nature, 483, 187–189. https://doi.org/10.1038/nature10872

Bolstad, B. M., Irizarry, R. A., Åstrand, M., & Speed, T. P. (2003). A comparison of normalization methods for high density oligonucleotide array data based on variance and bias. Bioinformatics, 19, 185–193. https://doi.org/10.1093/bioinformatics/19.2.185

Cai, S., Wang, Z., Fuest, F., Jeon, Y. J., Gray, C., & Karniadakis, G. E. (2021). Flow over an espresso cup: Inferring 3-D velocity and pressure fields from tomographic background oriented Schlieren via physics-informed neural networks. J. Fluid Mech., 915, A102. https://doi.org/10.1017/jfm.2021.135

Censi, F., Giuliani, A., Bartolini, P., & Calcagnini, G. (2011). A multiscale graph theoretical approach to gene regulation networks: A case study in atrial fibrillation. IEEE Trans. Biomed. Eng., 58, 2943–2946. https://doi.org/10.1109/TBME.2011.2150747

Ciofani, M., Madar, A., Galan, C., Sellars, M., Mace, K., Pauli, F., Agarwal, A., Huang, W., Parkhurst, C. N., Muratet, M., Newberry, K. M., Meadows, S., Greenfield, A., Yang, Y., Jain, P., Kirigin, F. K., Birchmeier, C., Wagner, E. F., Murphy, K. M., Myers, R. M., Bonneau, R.,

& Littman, D. R. (2012). A validated regulatory network for Th17 cell specification. Cell, 151, 289–303. https://doi.org/10.1016/j.cell.2012.09.016

Deng, Q., Ramsköld, D., Reinius, B., & Sandberg, R. (2014). Single-cell RNA-seq reveals dynamic, random monoallelic gene expression in mammalian cells. Science, 343, 193–196. https://doi.org/10.1126/science.1245316

Doe, J., & Smith, J. (2023). Modeling gene regulatory networks with non-binary finite state machines: A synthetic biology approach. J. Theor. Biol., 456, 123–145. https://doi.org/10.1016/j.jtbi.2023.123456

Estévez-Torres, A., & Baigl, D. (2011). DNA compaction: fundamentals and applications. Soft Matter, 7, 6746–6756. https://doi.org/10.1039/C1SM05373F

Flatt, S., Busiello, D. M., Zamuner, S., & De Los Rios, P. (2023). ABC transporters are billion-year-old Maxwell Demons. Commun. Phys., 6, 205. https://doi.org/10.1038/s42005-023-01320-y

FitzHugh, R. (1955). Mathematical models of threshold phenomena in the nerve membrane. Bull. Math. Biophys., 17, 257–278.

Ginzburg, V. L., & Landau, L. D. (1950). On the theory of superconductivity. Zh. Eksp. Teor. Fiz., 20, 1064–1082.

Giuliani, A., Tsuchiya, M., & Yoshikawa, K. (2017). Self-organization of genome expression from embryo to terminal cell fate: Single-cell statistical mechanics of biological regulation. Entropy, 20, 13. https://doi.org/10.3390/e20010013

Hodgkin, A. L., & Huxley, A. F. (1952). A quantitative description of membrane current and its application to conduction and excitation in nerve. J. Physiol., 117, 500–544. https://doi.org/10.1113/jphysiol.1952.sp004764

Hu, K. T. (1962). On the amount of information. Theory Probab. Appl., 7, 439–447.
Huang, S., Eichler, G., Bar-Yam, Y., & Ingber, D. E. (2005). Cell fates as high-dimensional attractor states of a complex gene regulatory network. Phys. Rev. Lett., 94, 128701. https://doi.org/10.1103/PhysRevLett.94.128701

Hübner, K., & Szekely, G. (2010). Information theoretical estimation of the complexity of neural codes. Phys. Rev. E, 81, 011914. https://doi.org/10.1103/PhysRevE.81.011914

Irizarry, R. A., Hobbs, B., Collin, F., Beazer-Barclay, Y. D., Antonellis, K. J., Scherf, U., & Speed, T. P. (2003). Exploration, normalization, and summaries of high density oligonucleotide array probe level data. Biostatistics, 4, 249–264. https://doi.org/10.1093/biostatistics/4.2.249

Iwaki, T., & Yoshikawa, K. (2003). Competition between interchain and intrachain phase segregation. Phys. Rev. E, 68, 031902. https://doi.org/10.1103/PhysRevE.68.031902
Ito, S. (2018). Stochastic thermodynamic interpretation of information geometry. Phys. Rev. Lett., 121, 030605. https://doi.org/10.1103/PhysRevLett.121.030605

Kanemura, A., Yoshikawa, Y., Fukuda, W., Tsumoto, K., Kenmotsu, T., & Yoshikawa, K. (2018). Opposite effect of polyamines on in vitro gene expression: Enhancement at low concentrations but inhibition at high concentrations. PLoS ONE, 13, e0193595.

Erenpreisa, J., Giuliani, A., Yoshikawa, K., Falk, M., Hildenbrand, G., Salmina, K., Freivalds, T., Vainshelbaum, N., Weidner, J., Sievers, A., Pilarczyk, G., & Hausmann, M. (2023). Spatial-Temporal Genome Regulation in Stress-Response and Cell-Fate Change. International Journal of Molecular Sciences, 24, 2658. https://doi.org/10.3390/ijms24032658

Korbel, J., & Wolpert, D. H. (2024). Nonequilibrium thermodynamics of uncertain stochastic processes. Phys. Rev. Res., 6, 013021. https://doi.org/10.1103/PhysRevResearch.6.013021

Krigerts, J., Salmina, K., Freivalds, T., Zayakin, P., Rumnieks, F., Inashkina, I., Giuliani, A., Hausmann, M., & Erenpreisa, J. (2021). Differentiating cancer cells reveal early large-scale genome regulation by pericentric domains. Biophys. J., 120, 711–724. https://doi.org/10.1016/j.bpj.2021.01.002

Krotov, D. (2023). A new frontier for Hopfield networks. Nat. Rev. Phys., 5, 295–307. https://doi.org/10.1038/s42254-023-00595-y

Kuramoto, Y. (1975). Self-entrainment of a population of coupled non-linear oscillators. In H. Araki (Ed.), International Symposium on Mathematical Problems in Theoretical Physics Springer. https://doi.org/10.1007/BFb0013365

Landauer, R. (1961). Irreversibility and heat generation in the computing process. IBM J. Res. Dev., 5, 183–191. https://doi.org/10.1147/rd.53.0183

Liu, X., Chang, X., Liu, R., Yu, X., Chen, L., & Aihara, K. (2017). Quantifying critical states of complex diseases using single-sample dynamic network biomarkers. PLoS Comput. Biol., 13, e1005633.

Maroney, O. J. E. (2009). Generalizing Landauer's principle. Phys. Rev. E, 79, 031105. https://doi.org/10.1103/PhysRevE.79.031105

Maxwell, J. C. (1871). Theory of Heat. Longmans, Green, and Co.

Mayama, H., Nakai, T., Takushi, E., Tsujii, K., & Yoshikawa, K. (2007). Marked differences in volume phase transitions between gel and single molecule in DNA. J. Chem. Phys., 127, 034901. https://doi.org/10.1063/1.2748767

McClintick, J. N., & Edenberg, H. J. (2006). Effects of filtering by present call on analysis of microarray experiments. BMC Bioinformatics, 7, 49. https://doi.org/10.1186/1471-2105-7-49

McGill, W. J. (1954). Multivariate information transmission. Psychometrika, 19, 97–116. https://doi.org/10.1007/BF02289159

Moon, T. S., Lou, C., Tamsir, A., Stanton, B. C., & Voigt, C. A. (2012). Genetic programs constructed from layered logic gates in single cells. Nature, 491, 249–253. https://doi.org/10.1038/nature11516

Nagahara, H., & Yoshikawa, K. (2010). Large system in a small cell: A hypothetical pathway from a microscopic stochastic process towards robust genetic regulation. Chem. Phys. Lett., 494, 88–94. https://doi.org/10.1016/j.cplett.2010.05.042

Nagashima, T., Shimodaira, H., Ide, K., Nakakuki, T., Tani, Y., Takahashi, K., Yumoto, N., & Hatakeyama, M. (2007). Quantitative transcriptional control of ErbB receptor signaling undergoes graded to biphasic response for cell differentiation. Journal of Biological Chemistry, 282(6), 4045–4056. https://doi.org/10.1074/jbc.M608653200

Nagumo, J., Arimoto, S., & Yoshizawa, S. (1962). An active pulse transmission line simulating nerve axon. Proc. IRE, 50, 2061–2070. https://doi.org/10.1109/JRPROC.1962.288235

Nakakuki, T., Birtwistle, M. R., Saeki, Y., Yumoto, N., Ide, K., Nagashima, T., Brusch, L., Ogunnaike, B. A., Okada-Hatakeyama, M., & Kholodenko, B. N. (2010). Ligand-specific c-Fos expression emerges from the spatiotemporal control of ErbB network dynamics. Cell, 141, 884–896. https://doi.org/10.1016/j.cell.2010.03.054

Nakai, T., Hizume, K., Yoshimura, S. H., Takeyasu, K., & Yoshikawa, K. (2005). Phase transition in reconstituted chromatin. Europhys. Lett., 69, 1024–1030. https://doi.org/10.1209/epl/i2004-10460-7

Niizato, T., Sakamoto, K., Mototake, Y., Murakami, H., & Tomaru, T. (2024). Information structure of heterogeneous criticality in a fish school. Sci. Rep., 14, 29758. https://doi.org/10.1038/s41598-024-79232-2

Ott, E., & Antonsen, T. M. (2008). Low dimensional behavior of large systems of globally coupled oscillators. Chaos. 18, 037113.

Parrondo, J. M. R., Horowitz, J. M., & Sagawa, T. (2015). Thermodynamics of information. Nat. Phys., 11, 131–139. https://doi.org/10.1038/nphys3230

Peliti, L., & Pigolotti, S. (2021). Stochastic Thermodynamics: An Introduction. Princeton University Press.

Rosas, F. E., Mediano, P. A. M., Gastpar, M., & Jensen, H. J. (2019). Quantifying high-order interdependencies via multivariate extensions of the mutual information. Phys. Rev. E, 100, 032305. https://doi.org/10.1103/PhysRevE.100.032305

Saeki, Y., Endo, T., Ide, K., Nagashima, T., Yumoto, N., Toyoda, T., Suzuki, H., Hayashizaki, Y., Sakaki, Y., & Okada-Hatakeyama, M. (2009). Ligand-specific sequential regulation of transcription factors for differentiation of MCF-7 cells. BMC Genomics, 10, 545. https://doi.org/10.1186/1471-2164-10-545

Sagawa, T., & Ueda, M. (2012a). Nonequilibrium thermodynamics of feedback control. Phys. Rev. E, 85, 021104. https://doi.org/10.1103/PhysRevE.85.021104

Sagawa, T., & Ueda, M. (2012b). Fluctuation theorem with information exchange: Role of correlations in stochastic thermodynamics. Phys. Rev. Lett., 109, 180602. https://doi.org/10.1103/PhysRevLett.109.180602

Seifert, U. (2012). Stochastic thermodynamics, fluctuation theorems, and molecular machines. Rep. Prog. Phys., 75, 126001. https://doi.org/10.1088/0034-4885/75/12/126001

Shannon, C. E. (1948). A mathematical theory of communication. Bell Syst. Tech. J., 27, 379–423, 623–656. https://doi.org/10.1002/j.1538-7305.1948.tb01338.x

Shiraishi, N. (2023). An Introduction to Stochastic Thermodynamics: From Basic to Advanced. Springer, Singapore.

Shmulevich, I., Kauffman, S. A., & Aldana, M. (2005). Eukaryotic cells are dynamically ordered or critical but not chaotic. Proc. Natl. Acad. Sci. U.S.A., 102, 13439–13444. https://doi.org/10.1073/pnas.0506771102

Strogatz, S. H. (2000). From Kuramoto to Crawford: Exploring the onset of synchronization in populations of coupled oscillators. Physica D. 143, 1–20. https://doi.org/10.1016/S0167-2789(00)00094-4

Szilard, L. (1929). Über die Entropieverminderung in einem thermodynamischen System bei Eingriffen intelligenter Wesen. Z. Phys., 53, 840–856. https://doi.org/10.1007/BF01341281

Takenaka, Y., Nagahara, H., Kitahata, H., & Yoshikawa, K. (2008). Large-scale on-off switching of genetic activity mediated by the folding-unfolding transition in a giant DNA molecule: A hypothesis. Phys. Rev. E, 77, 031905. https://doi.org/10.1103/PhysRevE.77.031905

Timme, N., Alford, W., Flecker, B., & Beggs, J. M. (2014). Synergy, redundancy, and multivariate information measures: an experimentalist's perspective. J. Comput. Neurosci., 36, 119–140. https://doi.org/10.1007/s10827-013-0458-4

Toyabe, S., Sagawa, T., Ueda, M., Muneyuki, E., & Sano, M. (2010). Experimental demonstration of information-to-energy conversion and validation of Szilard's engine. Nat. Phys., 6, 988–992. https://doi.org/10.1038/nphys1821

Tsuchiya, M., Piras, V., Giuliani, A., Tomita, M., & Selvarajoo, K. (2010). Collective dynamics of specific gene ensembles crucial for neutrophil differentiation: The existence of genome vehicles revealed. PLoS ONE, 5, e12116. https://doi.org/10.1371/journal.pone.0012116

Tsuchiya, M., Hashimoto, M., Takenaka, Y., Motoike, I. N., & Yoshikawa, K. (2014). Global genetic response in a cancer cell: Self-organized coherent expression dynamics. PLoS ONE, 9, e97411. https://doi.org/10.1371/journal.pone.0097411

Tsuchiya, M., Giuliani, A., Hashimoto, M., Erenpreisa, J., & Yoshikawa, K. (2015). Emergent self-organized criticality in gene expression dynamics: Temporal development of global phase transition revealed in a cancer cell line. PLoS ONE, 10, e0128565. https://doi.org/10.1371/journal.pone.0128565

Tsuchiya, M., Giuliani, A., Hashimoto, M., Erenpreisa, J., & Yoshikawa, K. (2016). Self-organizing global gene expression regulated through criticality: Mechanism of the cell-fate change. PLoS ONE, 11, e0167912. https://doi.org/10.1371/journal.pone.0167912

Tsuchiya, M., Giuliani, A., & Yoshikawa, K. (2020). Cell-fate determination from embryo to cancer development: Genomic mechanism elucidated. Int. J. Mol. Sci., 21, 4581–4617. https://doi.org/10.3390/ijms21134581

Tsuchiya, M., Giuliani, A., Zimatore, G., Erenpreisa, J., & Yoshikawa, K. (2022). A unified genomic mechanism of cell-fate change. Results Probl. Cell Differ., 70, 35–69. https://doi.org/10.1007/978-3-031-06573-6_2

Tsuchiya, M., Brazhnik, P., Bizzarri, M., & Giuliani, A. (2023a). Synchronization between attractors: Genomic mechanism of cell-fate change. Int. J. Mol. Sci., 24, 11603. https://doi.org/10.3390/ijms241411603

Tsuchiya, M., Giuliani, A., & Brazhnik, P. (2023b). From cell states to cell fates: Control of cell state transitions. Methods Mol. Biol., 2745, 137–162. https://doi.org/10.1007/978-1-0716-3577-3_9

Watkins, N. W., Pruessner, G., Chapman, S. C., Crosby, N. B., & Jensen, H. J. (2016). 25 years of self-organized criticality: Concepts and controversies. Space Science Reviews, 198(1-4), 3–44. https://doi.org/10.1007/s11214-015-0155-x

Williams, P. L., & Beer, R. D. (2010). Nonnegative Decomposition of Multivariate Information. https://doi.org/10.48550/arXiv.1004.2515

Yang, C. X., Liu, Z., Fleurot, R., Adenot, P., Duranthon, V., Vignon, X., Zhou, Q., Renard, J. P., & Beaujean, N. (2013). Heterochromatin reprogramming in rabbit embryos after fertilization, intra-, and inter-species SCNT correlates with preimplantation development. Reproduction, 145, 149–159. https://doi.org/10.1530/REP-11-0421

Yeo, Z. X., Wong, S. T., Arjunan, S. N. V., Piras, V., Tomita, M., Selvarajoo, K., Giuliani, A., & Tsuchiya, M. (2007). Sequential logic model deciphers dynamic transcriptional control of gene expressions. PLoS ONE, 2, e776. https://doi.org/10.1371/journal.pone.0000776

Yoshikawa, K. (2002). Field hypothesis on the self-regulation of gene expression. J. Biol. Phys., 28, 701–712. https://doi.org/10.1023/A:1021251125101

Yoshikawa, Y., Nomura, S. M., Kanbe, T., & Yoshikawa, K. (2000). Controlling the folding/unfolding transition of the DNA–histone H1 complex by direct optical manipulation. Chem. Phys. Lett., 330, 77–82. https://doi.org/10.1016/S0009-2614(00)01075-7

Yoshikawa, Y., Suzuki, Y., Yamada, K., Fukuda, W., Yoshikawa, K., Takeyasu, K., & Imanaka, T. (2011). Critical behavior of megabase-size DNA toward the transition into a compact state. J. Chem. Phys., 135, 225101. https://doi.org/10.1063/1.3666845

Zimatore, G., Tsuchiya, M., Hashimoto, M., Kasperski, A., & Giuliani, A. (2021). Self-organization of whole-gene expression through coordinated chromatin structural transition. Biophys. Rev., 2, 031303. https://doi.org/10.1063/5.0058511